FILIPE MIGUEL TOMAZ MONTEIRO

Licenciado em Biologia

CHARACTERIZATION OF THE HAZARA VIRUS AND TICK CELL LINES INTERACTIONS TOWARDS CRIMEAN-CONGO HAEMORRHAGIC FEVER VIRUS CONTROL.

MESTRADO EM MICROBIOLOGIA MÉDICA

Universidade NOVA de Lisboa

Maio, 2022

FILIPE MIGUEL TOMAZ MONTEIRO

Licenciado em Biologia

CHARACTERIZATION OF THE HAZARA VIRUS AND TICK CELL LINES INTERACTIONS TOWARDS CRIMEAN-CONGO HAEMORRHAGIC FEVER VIRUS CONTROL.

MESTRADO EM MICROBIOLOGIA MÉDICA

Universidade NOVA de Lisboa

Maio, 2022

Characterization of the Hazara Virus and Tick cell lines interactions towards Crimean-Congo Haemorrhagic Fever Virus control

FILIPE MIGUEL TOMAZ MONTEIRO

Licenciado em Biologia

Orientador: Doutor Gonçalo Seixas, Investigador Júnior
Instituto de Higiene e Medicina Tropical,
Universidade Nova de Lisboa

Coorientador: Doutora Ana Gonçalves Domingos, Investigadora Auxiliar,
Instituto de Higiene e Medicina Tropical,
Universidade Nova de Lisboa

Júri

Presidente: Doutora Rita Sobral,
Professora Auxiliar, FCT-NOVA

Arguente: Doutora Maria João Alves
Investigadora Auxiliar, Centro de Estudos de Vetores e Doenças Infeciosas
Doutor Francisco Cambournac, INSA

Orientador: Doutor Gonçalo Seixas,
Investigador Júnior, Instituto de Higiene e Medicina Tropical

MESTRADO EM MICROBIOLOGIA MÉDICA
Universidade NOVA de Lisboa
Maio, 2022

Characterization of the Hazara Virus and Tick cell lines interactions towards Crimean-Congo Haemorrhagic Fever Virus control.

Acknowledgments

Firstly, I would like to acknowledge Dra. Ana Domingos, for the opportunity to integrate in this thesis, after my initially contact enquiring about future projects.

To my supervisor, Dr. Gonçalo Seixas I want to thank him for his tremendous patience to work with me and for his many teachings during this experiment. Gonçalo was always ready to come to the laboratory to rescue me, whenever I needed assistance.

To my co-supervisor, Dra. Ana Domingos, I would like to thank for all the help provided, and I´m especially grateful for the sweet threats she would often offer to us! I want to express my deepest gratitude for all the kind words of encouragement that, in the darkest hour, help me turn around and believe in myself.

To my second co-supervisor, Dr. Ricardo Parreira I must thank for all the effort and hours spent instructing me. I am undoubtably in debt for all the knowledge I received.

To the "Ticks" group, I say thank you for the hospitability and friendly work environment I felt throughout my workdays, that hugely help me! A special thanks to Dra. Sandra Antunes for always be ready to help me, and to Leonardo Moerbeck for lifting my days with fun!

Finally, to all the people I´ve meet at IHMT and were part of this incredible experience, either teachers, co-workers or friends. A special thanks to my virology teachers, who opened the world of Viruses to me.

A título pessoal, e como a minha pátria é a língua portuguesa, aqui vai:

Aos novos amigos que este mestrado gerou, obrigado pelo companheirismo e apoio durante esta fase. Aos meus amigos de longa data, estou grato por ainda estarem presentes depois de tantos anos a aturar-me, em especial à prima Carolina pelo seu carinho e apoio, e às minhas amigas do secundário pela sua energia contagiante. Um grande bem-haja ao meu Frisco por puder desabafar com ele e ter alguém com quem estar.

Um agradecimento especial e caloroso à minha família, que sempre esteve presente a suportar-me. Em especial ao meu avô, do qual me orgulho tanto, que sempre lutou para que pudéssemos ter aquilo que ele nunca teve.

E por último, mas não menos importante (convém sublinhar essa última parte), quero agradecer à minha mãe, que sempre esteve presente a torcer por mim e a apoiar-me, e é a primeira a estender-me a mão quando eu mais preciso. Um grande Bem Haja.

List of Communications

Poster presentation in national congress

Tomaz, F., Antunes, S., Parreira, R., Domingos, A., Seixas, G.," Characterization of Hazara virus infection in *Hyalomma lusitanicum* tick cell line." Poster ID: 185. National Congress of Microbiology and Biotechnology-MicroBiotec2. 23rd – 26th November 2021 (Online Web-conference)

Abstract

Crimean-Congo haemorrhagic fever virus (CCHFV) (*Nairoviridae, Orthonairovirus*) is a tick-borne virus that causes a severe disease with high mortality rates in humans and is classified as a biosafety level (BSL) 4 pathogen. This virus is mainly transmitted by *Hyalomma spp.* ticks and has been increasingly detected in Europe and other CCHFV-endemic areas. Since *H. lusitanicum* geographical distribution encompasses the Iberian Peninsula, where recent human cases of CCHFV disease have been detected, a more comprehensive understanding of the tick-virus interactions is needed to fully realize the role this vector plays in the (re)emergence of CCHFV. As showed in previous studies, Hazara virus (HAZV) is a valid surrogate model to study CCHFV under BSL2 conditions. The aim of this thesis was to establish and characterize the infection of three tick-derived cell lines - HLE/LULS42, HAECTVM9 and ISE6 - with HAZV to elucidate the dynamics of the infection (*in vitro*) in the vector. Tick cell lines were maintained in parallel with HAZV grown in Vero E6 and SW-13 cells. The three tick cell lines were infected with HAZV at different multiplicities of infection and had their supernatants retrieved at several time-points post infection and later processed for RNA extraction using tri-reagent. Viral RNA was quantified using an in-house designed quantitative reverse transcriptase polymerase chain reaction (RT-qPCR) using a TaqMan probe targeting a region of the S segment of HAZV genome. Results obtained demonstrate that a persistent infection is formed in all three cell lines, without hampering the *fitness* of the tick cells. The viral titres obtained by RT-qPCR provided an image of the kinetics of the infection and show a peak of viral genomes at approximately 7-8 days post-infection. The data also shows that HLE/LULS42 – HAZV infected cells produce higher values of viral titre in all the three cell lines studied, displaying a difference in the kinetics of viral replication. Future studies are warranted in HLE/LULS42 tick cell line to study the molecular mechanisms underlying the viral persistence without damaging the host. Altogether, this work provides critical knowledge in understanding the vector-pathogen interactions and will guide future studies towards prevention and treatment of poorly studied viral threats.

Keywords: Crimean-Congo haemorrhagic fever virus, Hazara virus, Nairoviruses, Tick cell lines, Tick-borne viruses, *H. lusitanicum*, One-step real-time RT-PCR

Resumo

O vírus da febre hemorrágica da Crimeia-Congo (CCHFV) (*Nairoviridae, Orthonairovirus)* é um vírus transmitido por carraças responsável por uma grave doença com elevada taxa de mortalidade em humanos e é classificado como agente patogénico de nível de biossegurança (BSL) 4. Este vírus é transmitido principalmente por carraças do género *Hyalomma spp*. e a sua deteção na Europa e outras áreas endémicas de CCHFV tem aumentado. Visto que, a distribuição geográfica de *H. lusitanicum* abrange a Península Ibérica, onde foram detectados casos recentes de infeção por CCHFV, é necessária uma compreensão mais detalhada das interações entre a carraça e o vírus para melhor compreender o papel que este vetor desempenha na (re)emergência de CCHFV. Estudos prévios com o vírus Hazara (HAZV), validaram este vírus como um modelo para estudar CCHFV em condições BSL2. Esta tese teve como objectivos, estabelecer e caracterizar a infecção por HAZ, em três linhagens celulares distintas de carraças - HLE/LULS42, HAECTVM9 e ISE6 – de modo a elucidar a dinâmica de infecção *(in vitro*) neste vetor. As linhas celulares de carraça foram mantidas, em paralelo, com células Vero E6 e SW-13. As três linhagens celulares de carraça foram infectadas com HAZV em diferentes multiplicidades de infecção e o seu sobrenadante foi recuperado em vários pontos temporais pós-infecção, sendo posteriormente processado para extração de RNA usando tri-reagente. O RNA viral foi quantificado por meio de uma nova reação em cadeia da polimerase via transcriptase reversa em tempo real (RT-QPCR), usando uma sonda TaqMan, complementar a sequencia específica do segmento S do genoma de HAZV. Os resultados obtidos, evidenciam a formação de uma infecção persistente, presente em todas as três linhagens celulares, sem prejudicar a sobrevivência das mesmas. Os títulos virais obtidos através de RT-QPCR revelam um pico na deteção de genomas virais, aproximadamente 7-8 dias após a infecção. Estes resultados demonstram igualmente que a linhagem celular HLE/LULS42, infetada com HAZV apresenta os valores de título viral mais elevado em todas as três linhagens celulares estudadas, indicando uma diferença na cinética de replicação viral. É necessário realizar estudos futuros, usando a linha celular HLE/LULS42, para uma melhor compreensão dos mecanismos moleculares implícitos na manutenção da persistência da infeção viral sem danificar o hospedeiro. Concluindo, este trabalho fornece novos dados para a compreensão das interações entre vetor e agente patogénico e permitirá realizar novo estudos para a prevenção e tratamento de ameaças virais.

Table of figures

Table of Tables

Abbreviations

BSL2	Biosafety level 2
BSL4	Biosafety level 4
CCHFV	Crimean-Congo haemorrhagic fever virus
cDNA	Complementary DNA
CMC	Carboxymethylcellulose
CPE	Cytopathic effect
cRNA	Complementary RNA
DNA	Deoxyribonucleic acid
dpi	Days post-infection
dsDNA	Double-stranded DNA
GCP	Glycoprotein precursor
HAZV	Hazara Virus
IFN	Interferon
IHMT	Instituto de Higiene e Medicina Tropical
MOI	Multiplicity of infections
NP	Nucleoprotein
PCR	Polymerase chain reaction
PFU	Plaque forming units
qPCR	Quantitative PCR
RdRp	RNA dependent RNA polymerase
RNA	Ribonucleic acid
RNP	Ribonucleoprotein
RT-QPCR	Quantitative reverse transcription PCR
TBV	Tick-borne virus

1.Introduction

1.1. Tick-borne virus

Arthropod-borne viruses is a term applied to designate any kind of virus that is transmitted by an arthropod vector. These viruses have the unique ability to infect both an invertebrate host – the vector – and a vertebrate host. Arboviruses can be transmitted by a variety of arthropods such as mosquitoes, ticks, sand flies and biting midges (Young et al., 2014). Several tick-borne viruses (TBV) have been (re)emerging in the past few years and are closely monitored. Many ticks act as an efficient vector of pathogens to not only humans but also to several wild animals and livestock leading to major health and economic problems. These viruses are transmitted by either hard (*Ixodidae)* or soft (*Agasidae*) ticks and are capable of replicating within tick cells before being transferred to a susceptible vertebrate host. The ticks act as reservoir host for TBV since these arthropods, once infected, produce high viral titres, usually without being susceptible to the disease, and are therefore responsible for the virus transmission (Labuda and Nuttall, 2004; Mansfield et al., 2017; Wikel, 2018). Ticks are regarded as competent vectors due to their physiological ability to acquire and being able to maintain and replicate the infectious agent, culminating in the transmission of the pathogen. Vector competence consists in a complex tick-virus relationship and is affected by intrinsic and extrinsic factors. Ticks display a remarkable capacity to be infected when feeding, on a non-viraemic host, in close proximity to others infected ticks feeding nearby. This viral transport mechanism is called *co-feeding* and displays the multifaceted relationship at the tick-host-virus interface (Hubálek and Rudolf, 2012; Kazimírová et al., 2017). TBV encompasses a wide range of viral families, each with theirs one characteristics and different tick vectors. The following section will focus solely on the etiological agent of Crimean-Congo haemorrhaging fever disease.

1.2. Crimean-Congo Haemorrhagic Fever Virus

Crimean-Congo haemorrhaging fever (CCHF) is a severe viral zoonosis caused by the Crimean-Congo haemorrhagic fever virus (CCHFV), a highly pathogenic tick-borne virus. Sporadic outbreaks usually occur throughout Africa, eastern Europe and some parts of Asia. However, recent outbreaks in western Europe (Portillo et al., 2021) confirms a more widespread geographical dispersion than initially predicted. Therefore, and considering the high mortality rates and its potential use as a bioterrorism weapon, CCHFV is considered a worldwide public health concern and, recently classified as an emerging tick-borne virus (Ergonul, 2012; Hawman and Feldmann, 2018; Mansfield et al., 2017; Mehand et al., 2018; Mertens et al., 2013).

1.2.1. Viral characteristics

CCHFV is a *Orthonairovirus* belonging to the *Nairoviridae* family from the *Bunyavirales* order. Members of the *Nairoviridae* family are negative-sense RNA viruses with 3 single-stranded RNA segments comprising their genome (Garrison et al., 2020). Serological relationships, based on antibody cross-reactivity, reveal seven distinct serogroups for Nairovirus. CCHFV encompasses the CCHF group, alongside with Hazara virus (Casals and Tignor, 1980; Lasecka and Baron, 2014). Virions of CCHFV contain a triparted genome consisting of the small (S), medium (M) and large (L) segments (Figure 1). As for all *Bunyavirales* members, the S segment encodes the nucleocapsid protein (NP), responsible for forming a complex with each RNA genome fragment in the virion the genomic ribonucleoprotein complex (RNP). The M segment encodes a polyprotein, the glycoprotein precursor (GPC), which will suffer proteolytic cleavage and be processed into two membrane glycoproteins G_N and G_C (and other non-structural glycoproteins). It is presumed that the G_N and G_C glycoproteins play a key role in mediating the recognition and binding process to cells receptors and equally in the virion fusion to the host membrane. Lastly, the L segment encodes the L-protein: the viral RNA-dependent RNA polymerase (RdRp). The CCFV virion has a spherical shape, having 80–120 nm in diameter, and possess a lipid envelop, covered with glycoprotein spikes (G_N and G_C) (Kuhn et al., 2016).

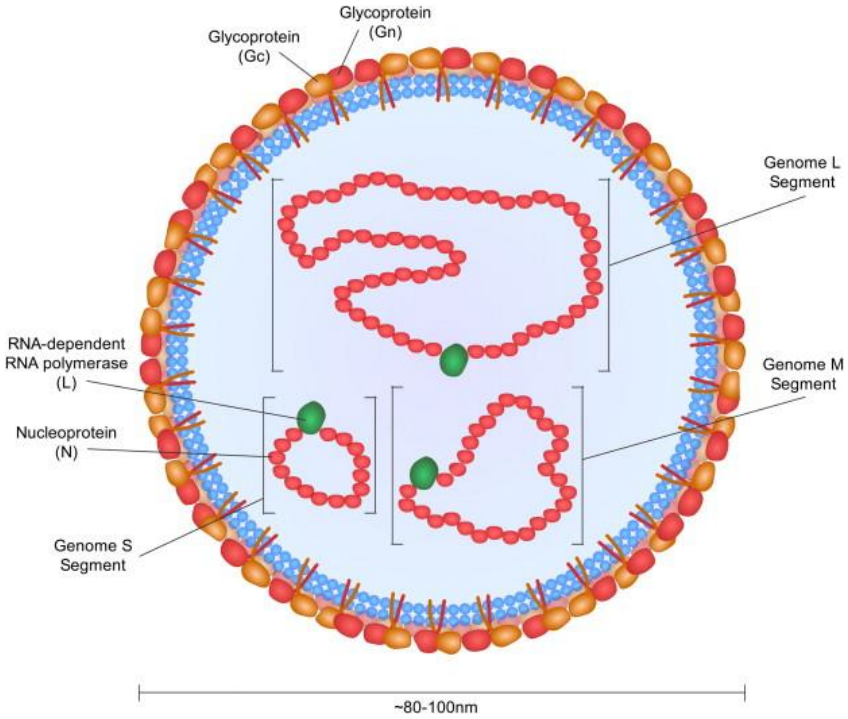

Figure 1. Schematic representation of the CCHFV virion. The CCHFV virion contains a tri-segmented, negative-sense, single-stranded RNA genome, encapsidaded by the nucleoprotein (NP) and the viral RNA-dependent RNA polymerase (RdRp) forming the genomic ribonucleoprotein complex (RNP). The lipid envelop is cellular membrane-derived and is studded with the glycoproteins G_N and G_C. Picture, with authorization, from Bente et al., (2013).

The replication cycle of this Nairovirus begins when the viral particle attaches to a currently unidentified host-cell surface receptor and is internalized via a clathrin-dependent process (Figure 2). The viral envelop fuses with the cell membrane triggering the release of the ribonucleoprotein complex, which is then uncoated granting access of the viral genome to the RdRp, responsible for transcribing CCHFV genome into viral mRNA. The virals mRNA´s encoding the nucleocapsid protein and the RdRp will be translated by the hosts ribosomes, while the polyprotein precursor of the membrane glycoproteins will be translated via endoplasmic reticulum-associated ribosomes and later undergoes processing forming the G_N and G_C glycoproteins which will be transported to the Golgi complex for maturation. As a result of the accumulation of the nucleoprotein in the cytoplasm, the viral genomic segments undergo an encapsidation process with the NP and L-protein and forms the RNP. The newly formed RNPs acquired a lipid envelop and the membrane surface glycoproteins at the Golgi complex leading into the budding and assembly of the CCHFV viral particles and subsequent release, by exocytosis, of the virion (Bente et al., 2013; Garrison et al., 2013; Zivcec et al., 2016).

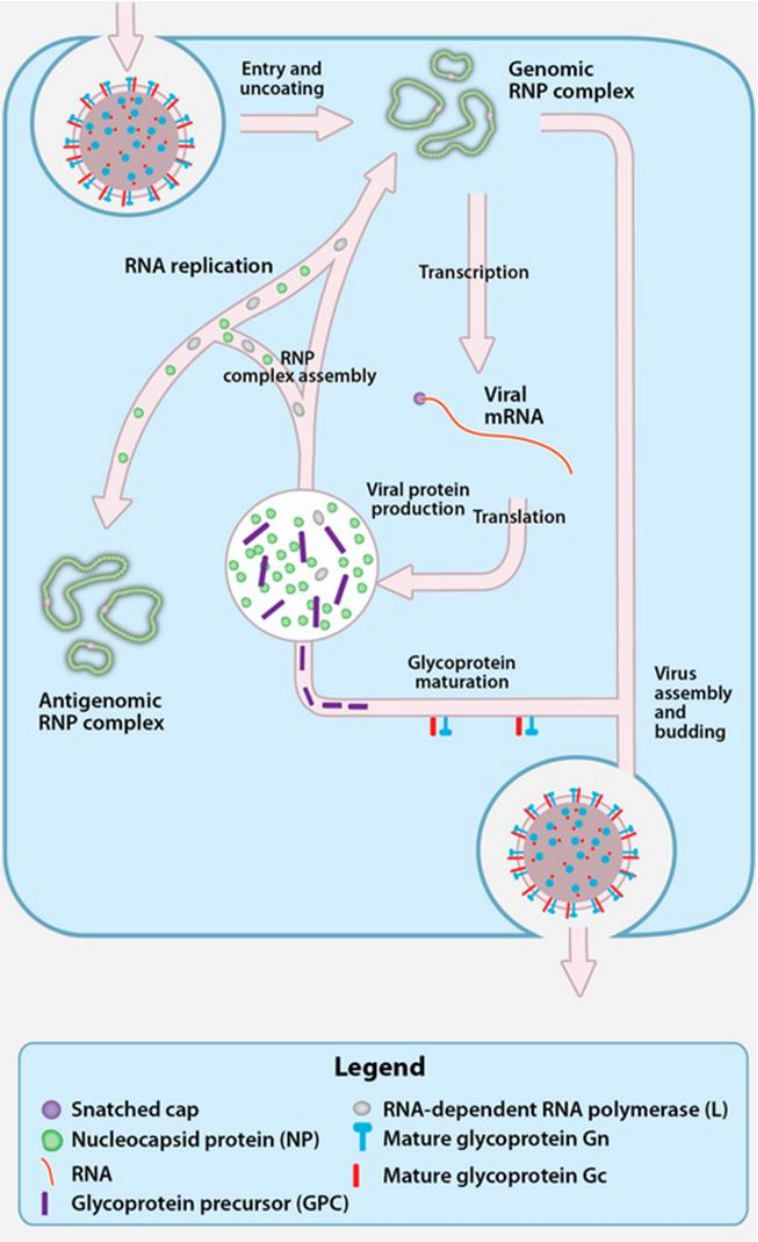

Figure 2. Schematic representation of CCHFV replication cycle. The CCHFV virions bind to an unidentified cellular receptor and is internalised via a clathrin-dependent manner. Fusion between the viral envelope and endosomal membranes triggers the uncoating of the viral genome and dissociation of the nucleocapsid. The viral genome is then transcribed into viral messenger RNA (mRNA). The viral mRNA is translated, by cytoplasmatic ribosomes, into the viral proteins (NP and RdRp). The glycoprotein precursor (GPC) is translated in the endoplasmic reticulum, later, is cleaved and undergoes processing and maturation in the Golgi apparatus rendering the Gn and Gc glycoproteins. At the same time, the NP and RdRp proteins form the RNP containing viral complementary RNA (cRNA), generated by the RdRp, forming the antigenomic RNP complex. The CCHFV virion is formed in the Golgi and exits the cell. Adapted from Zivcec et al., (2016).

1.2.2. Clinical analysis and pathogenicity of CCHFV

The first reported cases of CCHF date back to the summer of 1944 in, what was at the time, the soviet region of Crimea. The illness quickly developed into a haemorrhaging fever. It was only in 1965 that soviet researchers were able to isolate the etiological agent responsible for the 1944 Crimea illness, from blood samples collected from patients, and fully characterize the virus then named Drosdov strain (Hoogstraal, 1979). Later, in 1967, Antigenic Similarity between the Drosdov virus and a viral strain isolated from the Congo in 1956, also responsible for a haemorrhagic fever illness, was found. These results confirmed that the same etiological agent was responsible for the outbreaks, henceforth the viral agent would be classified as CCHFV (Casals, 1969).

Despite being associated with severe haemorrhagic fever disease, CCHF also quite often displays a milder symptomatology, such as non-specific febrile illness, muscular pain, vomiting weakness and others. Human infection with CCHFV is primarily associated with a tick bite, though contact with bodily fluids from infected animals or human patients can also lead to infection (Figure 3). There are described four different phases of CCHF in humans: incubation, pre-haemorrhagic, haemorrhagic and convalescent phases (Hoogstraal, 1979). The incubation period usually varies from 1-7 days. A sudden onset of fever accompanied by other non-specific symptoms (often headaches and vomiting) and an increasing viremia characterize the pre-haemorrhagic phase. Typically, after the 3rd – 5th day of disease the haemorrhagic phase begins with external haemorrhagic manifestations namely petechiae of the skin that often develops into large cutaneous ecchymoses (haematomas on mucous membranes of the skin) that are rare in other types of viral haemorrhagic fevers. Internal bleeding in the gastrointestinal system and urinary tract can lead ultimately to haemorrhagic shock and multi-organ failure resulting in death. The convalescent period for survivals may last up to one year until fully recovery from disease. The mortality rate of CCHF is generally cited as 30%. However, this number reflects mainly the known cases resulting from outbreaks and therefore may lack a wider sample of non-diagnosticated patients that displayed mild illness or were asymptomatic and thus were not properly identified and diagnosticated with CCHF (Bente et al., 2013; Blumberg et al., 2014; Whitehouse, 2004).

Previous studies have demonstrated a strong correlation between the viral load in patients and the outcome of disease. Reports show that high viral titres are detected in

patients with a fatal outcome accompanied with a poorly, if at all present, antibody response. Therefore, there is a strong relation between an increase in the viral replication and the severity of CCHF, which reflects an inability of the immune system to control the infection. In addition, the majority of haemorrhagic virus cause an extreme inflammatory response resulting in a dysregulation of cytokine (cytokine storm), which, allied with the inability of the immune system to properly organize an antibody response will lead to systemic shock and death (Saksida et al., 2010). The diagnostic of CCHF relies heavily on an appropriated epidemiological story, namely recent exposure history, together with physiological signs of the disease. The *gold standard* of diagnosis is to isolate the virus, but since CCHFV requires a biosafety level 4 laboratory (BSL4) to be handled it is considered an unpractical procedure. Currently, a molecular detection method for the viral genome is widely regarded as the fastest, safest, and most reliable diagnostic method. Other laboratory methods such a serological assays, namely enzyme-linked immunosorbent assays (ELISA), that detect human CCHFV-specific antibodies, may also be used.(Atkinson et al., 2012; Hawman and Feldmann, 2018).

1.2.3. Maintenance and vector transmission of CCHFV

The main vector of CCHFV are the hard ticks of the *Hyalomma* genus. Although CCHFV has been isolated in samples of over 30 distinct tick species, the detection of the virus in different ticks do not directly imply their involvement as an active and competent vector. As previously explained, a competent vector must be able to acquire the viral pathogen and maintain a life-long infection with considerable high viral titres enabling an efficient transmission to vertebrates (Bente et al., 2013). While even some soft ticks haven been shown to be infected with CCHFV *in vitro*, the virus itself is not able to induce a persistent infection and fails to be transmitted (Durden et al., 1993). Consequently, this large pool of arthropods detect with CCHFV surely reflects a recent ingestion of viremic vertebrate blood by the hematophagous arthropod or even a *co-feeding* scenario instead of a genuine persistent infection. Considering the strong correlation between the geographical range of confirmed cases of CCHFV infection

and the *Hyalomma* genus dispersion, it is predominantly accepted that *Hyalomma spp.* ticks are the only competent vector for CCHFV.

A tick must first be infected with CCHFV during a feeding process to establish itself as a possible vector for CCHFV transmission. Considering the life cycle of *Hyalomma spp.* ticks (see Figure 3), the infection process can be undertaken at the larvae, nymph, or adult stages. Therefore, there is a variety of opportunities for viral transmission either between the ticks themselves or between the tick and a vertebrate host. CCHFV is able to be transmitted not only vertically throughout the tick's life cycle between different life stages (transstadial transmission); and by the female to the eggs (transovarial transmission) but also horizontally, trough *co-feeding* to others ticks, and also to wild animals in the nature or domesticated animals (Spengler and Estrada-Peña, 2018; Xia et al., 2016). After infection, the virus must surpass several biological barriers within the tick before being able to be transmitted. CCHFV will first replicate in the midgut, following infection, and eventually will disseminate into the salivary glands where it will be able to be transmitted upon a tick bite, but it will also disseminate into the reproductive tissues allowing vertical transmission. It is precisely in the salivary glands and reproductive organs that the higher viral titres are achieved, however, this is linked primarily to the high tissue proliferation in those regions rather to an increased rate of virus replication (Dickson and Turell, 1992).

Despite the crucial role ticks play as vectors and natural hosts, vertebrates also have a significant role in the overall chain of CCHFV transmission. A vertebrate species not only supports the presence of ticks acting as a tick maintenance host, but also serve as a virus reservoir, enabling the maintenance of virus circulation in the wild (Gargili et al., 2017).

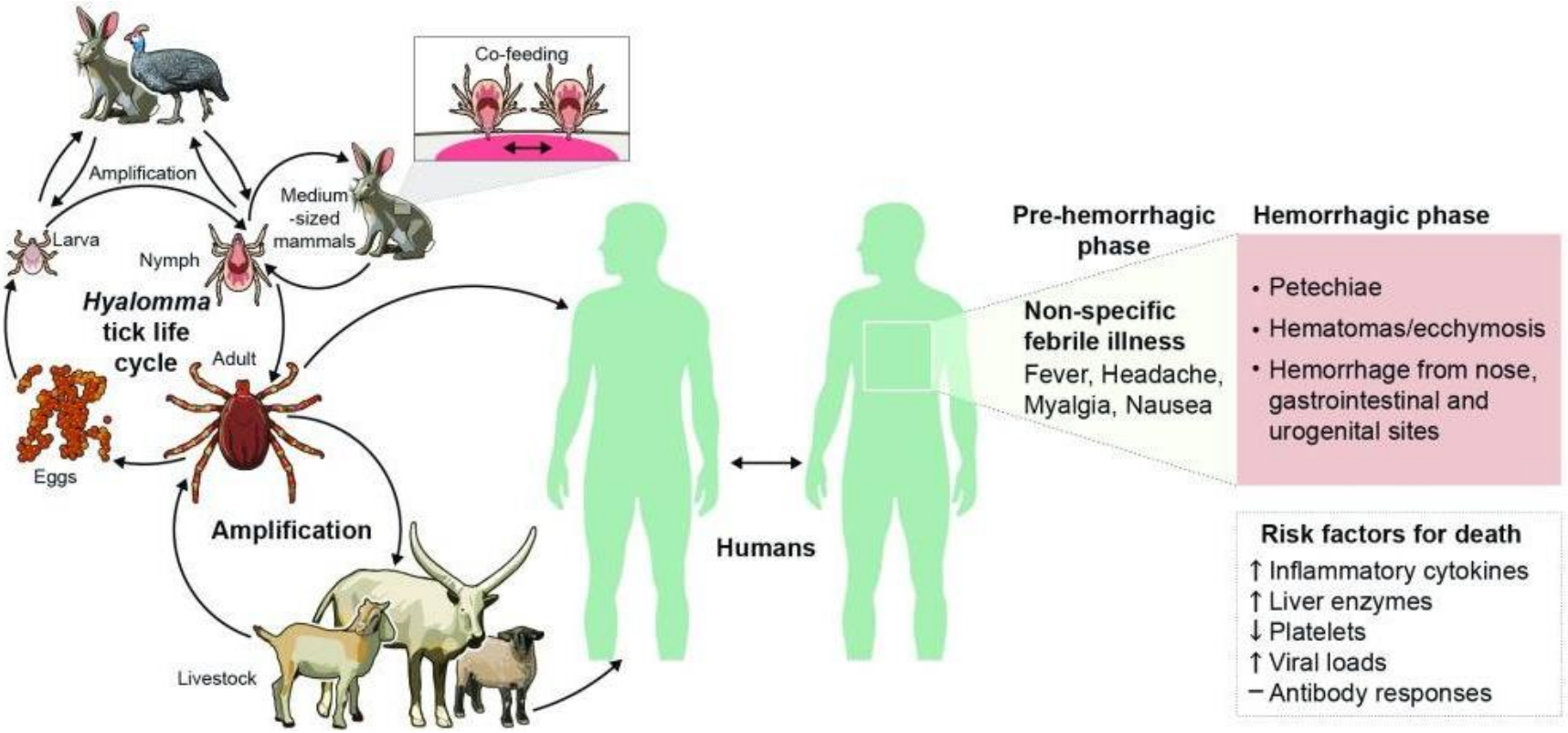

Figure 3. Life cycle of Hyalomma spp. ticks and infection routes for CCHFV transmission. *Hyalomma* genus ticks are the main vector for CCHFV. After hatching, the larvae find a suitable host for their blood meal, following engorgement the larvae either remains in the host and molt (two-host ticks), or falls of and molt on the ground (three-host ticks). The nymphs feed on the animal blood and after engorgement drops and molt on the ground. The adult tick then attaches to a new, bigger host (wild animals such as boars or deers, or domestic animals). The matting process happens on the host and afterwards the female tick lay the eggs. Transmission of the virus can occur at any stage. The ticks can become infected during a viremic meal feeding, or during *co-feeding.* Vertebrates act as amplifiers host for CCHFV. Humans can become infected directly through tick bite, from contacting with infected blood from animals, or during patient care (nosocomial transmission). Adapted from Hawman and Feldmann, (2018).

1.2.4. Geographical dispersion of CCHFV

CCHFV has been reported in several countries spanning a wide geographical range. The endemic regions of this virus can be aggregated into five main areas: eastern Europe, namely the Balkan area; most part of sub-Saharian Africa; the middle East and Turkey; eastern and central Asia, notably Pakistan and China; and more recently in some parts of southwestern Europe (Figure 4) (Hubálek and Rudolf, 2012; Palomar et al., 2017a; Portillo et al., 2021; Shahhosseini et al., 2021; Zhang et al., 2018). Despite the endemic foci of CCHFV in Europe is mainly associated with Eastern countries (such as Albania, Bulgaria, Greece and Kosovo), reports of CCHFV circulation in south westerns parts of Europe has been described (Portillo et al., 2021). Those appearances of CCHFV infections can be originated from either imported cases from endemic areas to Europe such as those registered in the UK, France and Germany (Shahhosseini et al., 2021; Spengler et al., 2019), or can be the result of a direct contact with the virus (autochthonous case) as described in Spain (Negredo et al., 2017; Anabel Negredo et al., 2021). Due to this emerging viral threat in southern Europe, this thesis will focus mainly on the Iberian Peninsula situation regarding CCHFV presence and dissemination.

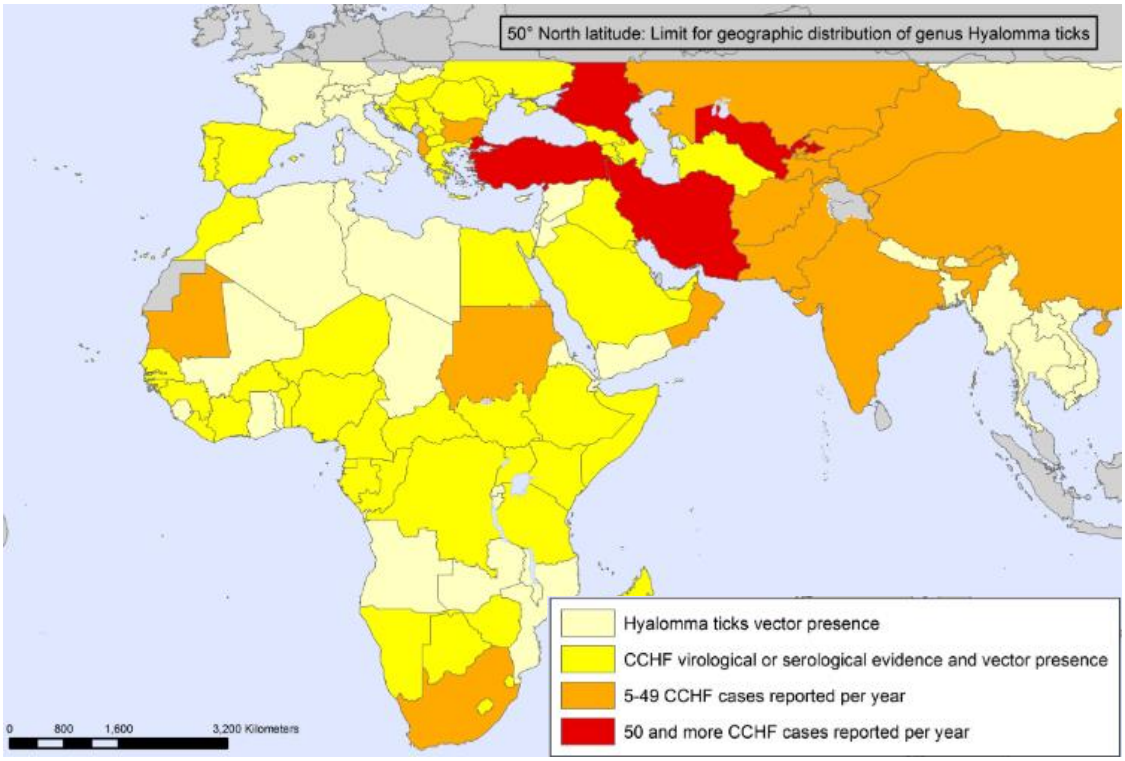

Figure 4. Geographical distribution of CCHFV. Countries in red have reported more than 50 cases of CCHF disease to the WHO per year, while those in coloured in orange reported fewer than 50 cases annually. The countries rendered in yellow have either a serological or virological evidence of CCHFV, despite not having any reported case. While coloured yellow, Spain has reported confirmed CCHF cases in the past 4 years. This figure is adapted from upon that displayed by the WHO (https://www.who.int/health-topics/crimean-congo-haemorrhagic-fever#tab=tab_1), originally from 2017.

1.2.5. The Iberian case

The Iberian Peninsula is situated on the westernmost point of Europe, has a moderated Mediterranean climate, suitable for a wide range of tick populations to persist. In Portugal, the latest report (2021), from the National Institute of Health, responsible for vector-borne diseases surveillance, reveals that there are currently in circulation 22 different tick species, namely *Hyalomma lusitanicum* (Koch, 1844) and *Hyalomma marginatum* (Koch, 1844) (Figure 5). Analysis on the *Hyalomma spp.* ticks collected either from parasitising cattle and wild animals or harvest in nature (questing ticks) revealed no sign of CCHFV. This report also highlighted that *Hyalomma spp.* ticks are predominantly found in the south region of Portugal, being adapted to the high temperatures and relatively low humidity values registered in the region (Centro de Estudos de Vetores e Doenças Infeciosas Doutor Francisco Cambournac, 2022). In Spain, multiple studies also attest the presence of both Hyalomma genus ticks throughout the entire country, notably in the central and southeast regions, although a significant increase in their abundancies has been observed in the past few years (Barandika et al., 2011; Vieira Lista et al., 2022). Furthermore, studies have revealed that *H. lusitanicum* is better suited to the Mediterranean basin climate and vegetation, being able to support the high temperatures in summer accompanied with long periods of low humidity and scarce rainfall (Barandika et al., 2011). It is established that the Iberian Peninsula possess the ecological conditions to support populations of CCHFV vector. In addition, migratory birds may play a role in virus dissemination over large distances, by carrying CCHFV-infected ticks (Portillo et al., 2021). Climate change may equally have an influence in exacerbating the spread of CCHFV to new regions since it can alter not only bird migration routes but also influence tick seasonal and facilitate the spread to new regions.

The detection of CCHFV in the Iberian Peninsula was first reported in 2010 in *H. lusitanicum* ticks collected from adult red deer (*Cervus elaphus*) in the Cáceres region of Spain, close to the Portuguese border (Estrada-Peña et al., 2012). Previously, CCHFV antibodies were found in six people in the Cuba region of Portugal, in a serological survey conducted in 1985. The survey revealed strong evidence of human contact with the virus which may be present focally in some regions of southern Portugal, although, the virus itself was not isolated (Filipe et al., 1985). Since those first serological studies in 1985 there are no reported findings of CCHFV in Portugal, neither in ticks, animals or humans. However, no epidemiological update, either of

serological prevalence or viral screening in ticks has been employed at large scale in Portugal ever since. Regarding Spain situation, in addition to the first report of CCHFV in 2010, several studies have been conducted in order to properly understand the circulation of CCHFV in Spain (Portillo et al., 2021). As a follow-up to the 2010 CCHFV discovery in Cáceres, phylogenetics analysis on the possible origin of the virus demonstrated that the viral strain isolated showed a closer affinity with African clades rather than to strains commonly found in Eastern Europe, suggesting a West African origin for the CCHFV circulating (Cajimat et al., 2017). These findings further corroborate the hypothesis that migratory birds coming from Western African countries may act as a gateway to introduce CCHFV in Southern European countries. Migratory birds have been found to be host of immature stages of *Hyalomma* ticks. A study on ticks collected from migratory birds in Morocco, all classified as *H*. *marginatum*, discovered CCHFV in three tick pools. This clearly demonstrates that migratory birds possess the potential for viral dispersion. Furthermore, the genetic analysis of the isolated CCHFV sequences showed a 100% identical match with the Sudanese AB1-2009 strain and the Mauritania ArD39554 strain, likewise the Moroccan isolate displayed a 98.9% identity with the CCHFV sequence isolated in Cáceres (Palomar et al., 2013). A similar study conducted in Spain also collected *H*. *marginatum* ticks from migratory birds from various Spanish regions, but it failed to detect CCHFV (Palomar et al., 2016). Since those early findings several studies have been conducted in Spain showing a widespread detection of CCHFV in ticks (mainly *H. lusitanicum)*, throughout the country, whether having been gathered in natured or collected feeding in wild or domesticated animals (Cajimat et al., 2017; Moraga-Fernández et al., 2021; Negredo et al., 2019; Palomar et al., 2017b; Sánchez-Seco et al., 2022). Therefore, it is proven that, although *H*. *marginatum* is credited with being the most important vector for CCHFV transmission, new data from Iberian Peninsula clearly demonstrate the importance of *H. lusitanicum* as a putative vector of CCHFV endemicity in the region.

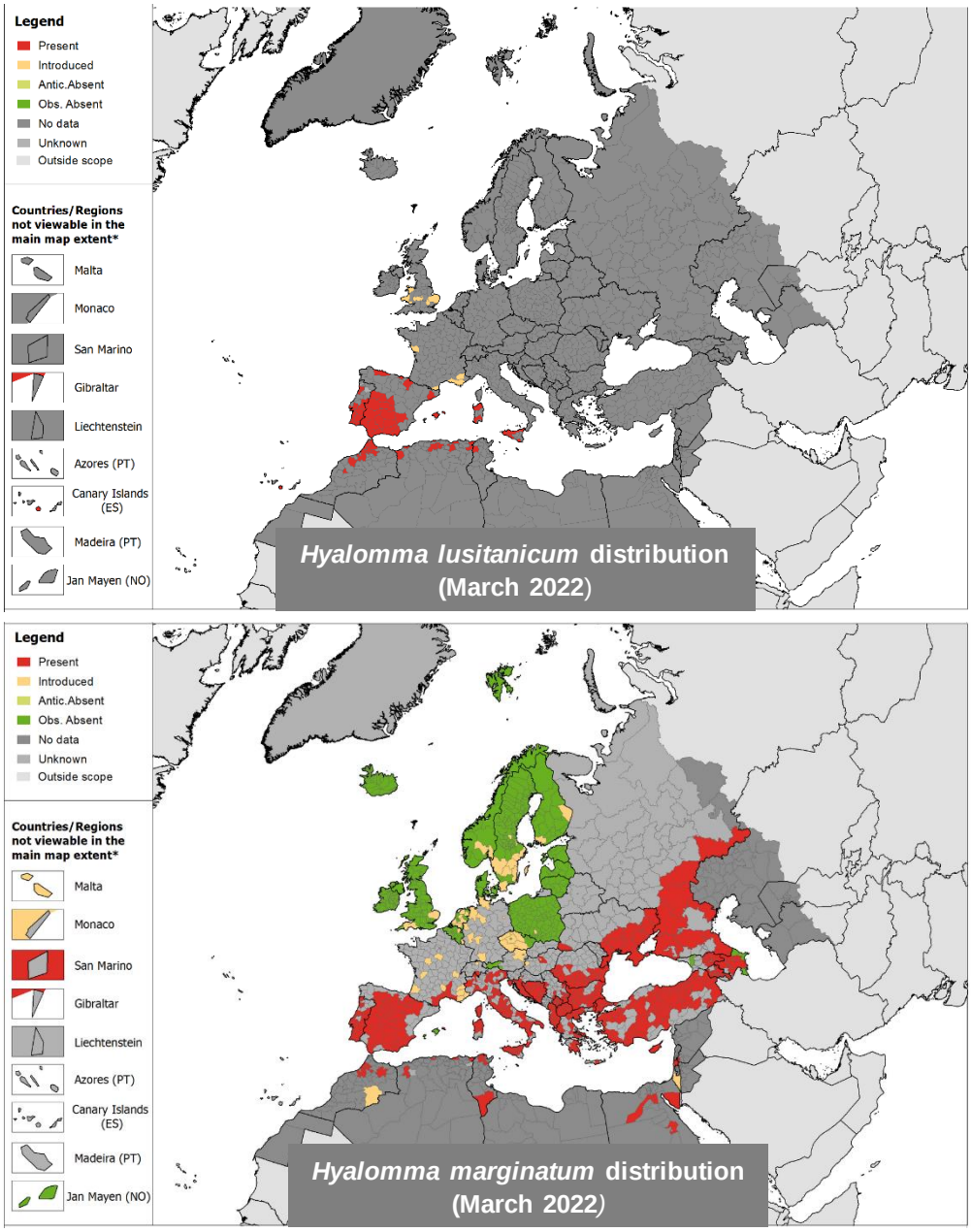

Figure 5. Distribution of H. lusitanicum and H. marginatum across Europe. Represented in red are the regions where the ticks have been found. Yellow areas showcase regions where the vector was detected, without yet confirmed establishment of population. The green regions indicated no presence of the corresponded tick. This figure was adapted from information available from the European Centre for Disease Prevention and Control, accessible at: https://www.ecdc.europa.eu/en/disease-vectors/surveillance-and-disease-data/tick-maps.

The first detectable human infection case with CCHFV in southern Europe was reported in 2016 in Ávila province, in Castile-León (central Spain). result of a tick bite, and later died. The healthcare worker responsible for the patient was also infected (nosocomial infection), but recovered (Negredo et al., 2017). Since 2016, seven other people have become infected with CCHFV, all of them infected through a tick bite. All of those cases were also reported in the central region of Spain and in close proximity with the Portuguese border (Arteaga et al., 2021; Negredo et al., 2021). Following an investigation on a 2013 patient who recovered from a severe infection caused by a tick bite in the aforementioned high-risk exposition areas, it was discovered a retrospective identification of an autochthonous case (Ana Negredo et al., 2021). These findings bring to light the importance of immunological surveys which may allow a more rigorous idea of the full extent of circulation of CCHFV in Spain. Before the onset of CCHFV infections in Spain, serological studies performed in people at risk of being bitten by ticks showed no antibodies against CCHFV in the serum samples analysed (Palomar et al., 2017b). Despite that, a sero-surveilhance study carried out in blood-donors in 2017-2018 presented a seroprevalence between 0,58% and 1,16% in analysed samples. The data points to the possibility of CCHFV circulation in individuals without presenting any symptomatology and represents a new insight into the epidemiology of CCHFV circulation in Spain (Arteaga et al., 2020). The findings also exacerbate the urgency of more extensive studies such as CCHFV screening in ticks and seroprevalence studies not only in humans living in areas on emerging foci endemicity for this virus (in Spain as well as Portugal) but also on wild and domestic animals that have a greater chance of being bitten by infected ticks and acquiring antibodies against CCHFV.

1.2.6. Animal models and tick-derived cell lines for CCHFV research

Unlike most haemorrhagic fever virus, CCHFV has repeatedly demonstrated, in numerous studies, that does not cause any clinical features of disease in immunocompetent commonly used animal species, despite being able to be infected by CCHFV and develop viremia (Garrison et al., 2019; Hawman and Feldmann, 2018;

Hoogstraal, 1979). As a result of this, for many years, the only available animal model suitable for research on this *orthonairovirus* were neonatal mice or rats, whose absence of a functional immune system enable the onset of disease. However, this model has its limitations as it does not allow pathogenic studies of CCHF disease neither immunity mechanisms. Such restrictions have hampered CCHFV research, namely on evaluating potential vaccine candidates (Garrison et al., 2019; Mendoza et al., 2018; Mertens et al., 2013). A study on the role of the innate immunity against CCHFV infections found that type I interferon-α (IFN) is capable of inhibiting viral replication making this intrinsic cellular resistance factor a key player in controlling infection (Andersson et al., 2006). Combining the new knowledge on the role of IFN in the outcome of CCHFV infection, a new mouse strain, lacking the type-I IFN receptor (A129) was developed. This new animal model revealed to be highly susceptible to CCHFV infection (Bereczky et al., 2010). Furthermore, a different knockout mice model was tested, having a deficient on the STAT-1 signalling molecule exhibiting restrictive response to all the three types of IFNs (Bente et al., 2010). The absence of intracellular IFN response present on STAT-1 knockout mice leads some to considerate the A129 mice a more suitable model for vaccine development studies against CCHFV (Dowall et al., 2017). A study conducted with non-human primates describe a possible novel animal model for CCHFV. Cynomolgus macaques (*Macaca fascicularis*) were infected with CCHFV (isolated from a human clinical case) and developed a clinical outcome similar to the human manifestations of CCHF (Haddock et al., 2018). This newly discovered animal model has the potential to be applied in vaccine studies and the screening for possible antivirals and therapeutic options. In fact, a DNA-based vaccine was tested on cynomolgus macaques providing a significant protection against CCHFV (David W. Hawman et al., 2021). Recent reports have also described a novel variant of CCHFV (created by serial passage of CCHFV strain Hoti in mice livers) capable of replicating to high viral titres and causing disease in immunocompetent mice (Hawman et al., 2021)

In the past few years, novel research approaches have raised using tick-derived cell lines as an *in vitro* model to study viral replication, infection control responses and tick-virus interactions. Tick cell lines tolerate being infected with a tick-borne virus, without showing any cytopathic effect (Talactac et al., 2021; Wikel, 2018). The contrast of behaviour displayed by tick cell lines upon infection with virus has sparked an interest in studying this innate tick immunity and open possibilities for CCHFV research.

Especially, characterizing tick-antiviral responses mechanisms to infection may lead to validate possible pathways for viral replication hampering and extrapolate the new findings to a mammalian model (Hart and Thangamani, 2021). Tick-derived cell lines serve not only to isolate and propagate viral agents but also play a key role in pathogen-host interaction studies, namely genomics, transcriptomics and proteomics system studies (Al-Rofaai and Bell-Sakyi, 2020; Bell-Sakyi et al., 2007). Regarding CCHFV, previous study conducted to assess the susceptibility of different tick cell lines to infection revelled a clear preference for *Hyalomma anatolicum* derived cell lines (HAE/CTVM8 and HAE/CTVM9) (Bell-Sakyi et al., 2012). These cell lines are widely used whenever an *in vitro* study using tick-derived cell lines and CCHFV is carried out (Salata et al., 2018).

1.3. Hazara Virus

Due to CCHFV high pathogenicity and absence of specific treatment or preventive vaccine, manipulation and handling of this *Orthonairovirus* must be conducted under a Biosafety level four (BSL4) containment level. The scarcity of such expensive laboratory conditions, especially in the regions where CCHFV is endemic, has led to the adoption of a BSL2 surrogate Nairovirus model.

Hazara virus (HAVZ) was first isolated in west Pakistan from *Ixodes redikorzevi* ticks (Begum et al., 1970). Evidence shows that HAZV is closely related to CCHFV as both viruses are antigenically related, being both members of the same serogroup (Casals and Tignor, 1980, 1974). HAZV shares the same virion characteristic as CCHFV, see Figure 1. HAZV is currently classified as a *Orthonairovirus* member of the *Nairoviridae* family (such as CCHFV). Since HAZV is non-pathogenic to humans, can be manipulated under BSL2 conditions. Addressing the use of HAZV as a possibly surrogate model for CCHFV research, a study conducted using IFN type I receptor-knockout mice infected with HAZV displayed signs of pathogenicity associated with the virus. Infection with HAZV in the immunocompromised mice resulted in severe disease and death (Dowall et al., 2017), as already observed with CCHFV infection (Bereczky et al., 2010). These findings have potentiated the use of HAZV as a surrogate model

for CCHFV research conducted under BLS2 conditions and, nowadays, HAZV is widely used and regarded as a valid surrogate model for research (Molinas et al., 2016; Monteil et al., 2020; Surtees et al., 2016).

Although several studies had already studied HAZV infection in tick and mammalian cells lines, there was no quantitative reverse transcription PCR (RT-qPCR) using probe methodology described in the literature in use at the time of the developing stage of this work (Flusin et al., 2011; Fuller et al., 2019a, 2019b; Garcia et al., 2005). It was decided then, that for a matter of simplification and cost-reduction this work would design a new RT-qPCR assay enabling both the detection and quantification of HAZV genomic material directly from RNA, previously isolated, and extracted from the infected cell. This method enables to directly determine the loads of viral genome equivalent in the samples, facilitating the process of evaluating the development of infection in tick cell lines. Furthermore, using a reverse-transcription methodology allows to remove the cDNA conversion (of the extracted RNA) step, decreasing any loss of genetic material during those processes. During this work, two independent studies using a RT-qPCR protocol for detection of HAZV were published (Hartlaub et al., 2020; Monteil et al., 2020) yet both studied HAZV infection in mammalian cell lines. Despite this, it was decided to finish the development of this TaqMan® based RT-qPCR assay and to use it to detect and quantify HAZV viral material not only in mammalian cells but also in tick-derived cell lines.

1.4. Molecular methods for viral detection

1.4.1. Conventional polymerase chain reaction

The polymerase chain reaction (PCR) is a enzymatic amplification of DNA *in vitro*, and is widely regarded as a key tool for detecting a broad range of templates (nucleic acids) in multiple scientific research, namely virology (Clementi et al., 1993; Kralik and Ricchi, 2017; Mackay et al., 2002). This method uses primers (synthetic oligonucleotides) which will hybridize, through complementary base pairing, to a specific target sequence in the DNA template, the primer-template hybrid complex will act as a subtract for the

DNA polymerase, which will create a new complementary strand, to the target sequence, by addiction of deoxynucleotides, resulting in the final product – amplicon. (Jalali et al., 2017; Mackay et al., 2002). Traditional PCR involves three steps: (1) denaturation, allowing the double-stranded DNA (dsDNA) to separate its double helix structure; (2) annealing, which allows for primer annealing and (3) extension where the DNA polymerase synthetizes the new DNA strand; which repeat themselves (30-40 cycles). As in each cycle the DNA amount approximately doubles, this method results in an exponential increase of DNA. Although conventional PCR is still extensively used in multiples research it only allows to visually detect a targeted region of interest.

1.4.2. Quantitative polymerase chain reaction

A variation of this method, the quantitative PCR (qPCR) became increasingly used as it not only allows for the detection of the specific region of interest, but it can also quantify the DNA as the reaction progress allowing to determine the copy number of the sequence of interest. Quantitative PCR is capable of monitoring the DNA amplification in real time by measuring the level of fluorescence, enabling a correlation between the fluorescence concentration and the PCR product concentration.(Adams, 2020; Mosammaparast and McAdam, 2013).

When preparing a qPCR assay it is of most importance to decide on the fluorescent-based methods which will be applied for nucleic acid analysis. The fluorogenic mechanisms to induce fluorescence vary, however these can be distinguished between DNA binding dyes and fluorophore-labelled oligonucleotides (Figure 6) (Navarro et al., 2015). Fluorescent DNA binding dye will bind non-specifically to dsDNA, resulting in an increase of fluorescence proportionally to the concentration of PCR product, measured in the extension phase of each cycle of qPCR. The most commonly used DNA intercalating binding dye is SYBR Green. SYBR Green will bind to any dsDNA, which includes primer-dimers (non-specific products that will emit fluorescence). Hence, a *melt curve* is necessary to validate the results whenever using any DNA binding bye. This will guarantee that the product of fluorescence comes from a specific product. As dsDNA of different lengths will melt at different temperatures the temperature gradient step, of which consists of a *melt-curve*, will allow to distinguish between the specific

amplicons of interest (intercalated with SYBR Green) and others non-specific products as primer-dimers (Adams, 2020; Jalali et al., 2017; Mosammaparast and McAdam, 2013).

The second method of detection of fluorescence is by using hydrolysis probes such as TaqMan probes. Hydrolysis probes are oligonucleotides containing a Fluorophore, a small fluorescent molecule that are attached to oligonucleotide at the 5′-end, and a quencher at the 3′-end that acts as an acceptor of fluorescence. As the names indicates a quencher is a molecule that quenches the fluorescence generated by the donor fluorescent molecules when in close proximity (Holland et al., 1991). The 5'- 3'-exonuclease activity of DNA polymerase enables the cleavage of the probe during the extension step therefore resulting in an emission of fluorescence. Considering that the probe is designed to bind specifically to the interested targeted DNA region, a TaqMan assay is much more sensitive and specific than intercalating dyes (Adams, 2020; Kutyavin et al., 2000; Navarro et al., 2015). Currently, qPCR´s using TaqMan probe as the detection method have become widely use in virology, since this methodology can be used either in single or multiplex formats and provides a rapid and specific virus detection method (Cui et al., 2022; Drosten et al., 2002; Garrison et al., 2007).

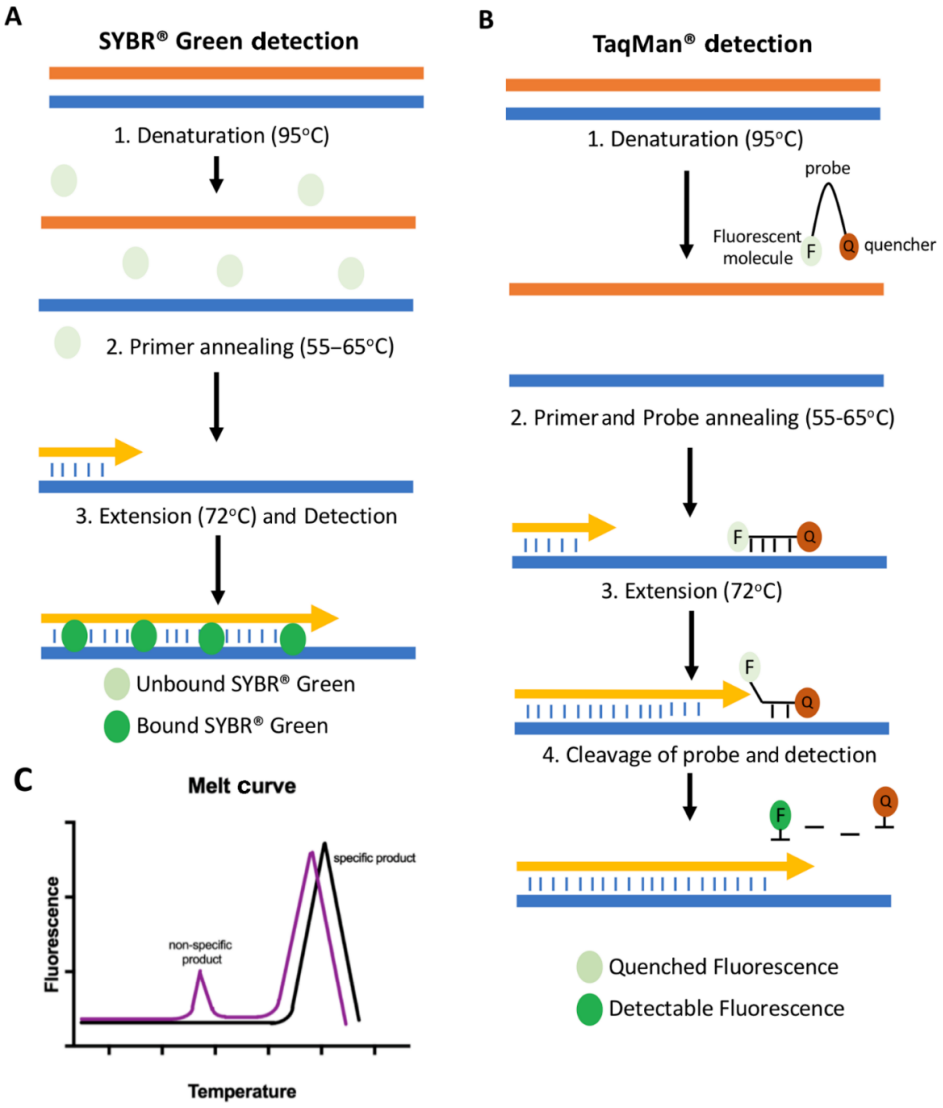

Figure 6. Representation of the mechanism of action of SYBR Green dye and TaqMan probe. A - SYBR Green is a DNA binding dye, which means that it binds to dsDNA. During the extension step, the DNA polymerase synthetizes the new complementary DNA chain, leading to the formation of dsDNA. SYBR Green dye will bind to the newly formed dsDNA and emit fluorescent. While more dsDNA is formed at each amplification cycle, more will the fluorescent emitted from the dye increase. C - As SYBR Green binds to any dsDNA molecule, after the qPCR assay it is custom to generate a melt-curve which will enable the user to distinguish between non-specific products generated (such as Primer-Dimers), and the targeted product of interest (which displays a higher melting temperature). B - The TaqMan assay consists in the use of a hydrolysis probe, specifically design to complement the targeted region of interest. While intact, the probe is unable to emit fluorescent thanks to the proximity of a quencher that causes the dye signal to be quenched. However, during the polymerization of the DNA sequence by the DNA polymerase the probe is cleaved, and the fluorescent dye is liberated enabling it to emit detectable fluorescent. Due to the stringy complementarity of the probe and the targeted sequence, any fluorescent detected comes only from amplification of the targeted sequence. Adapted from Adams, (2020).

1.4.3. Quantitative reverse transcriptase polymerase chain reaction

Reverse transcription PCR (RT-PCR) enables the amplification of RNA targets. In RT-PCR, the RNA will be the template for the reverse transcriptase enzyme to generate a single-stranded copy of complementary DNA (cDNA), which later is amplified by a DNA polymerase resulting in double-stranded cDNA, used as a template into a standard PCR process (Clementi et al., 1993; Jalali et al., 2017). The real-time reverse transcription polymerase chain reaction (RT-qPCR) enables the use of a fluorescence-based quantitative assay (qPCR) to measure RNA levels, allowing rapid detection and analysis of viral transcriptional activity. Therefore, the RT-qPCR is a quantitative and qualitative assay, frequently used for gene expression (Bustin, 2000). RT-qPCR represents a rapid and highly specific and sensitive method, broadly used in virology for CCHFV detection (Garrison et al., 2007; Koehler et al., 2018). In addition, RT-PCR can be undertaken in a one-step reaction or a two-step reaction. The main difference stands where the reaction itself takes place. A one-step RT-PCR is carried out in the same reactional tube and, therefore, the primers and probes are designed to detect specific sequences in viral genome. This method enables not only a more rapid assay but also minimizes sample handling, reducing pipetting error or cross-contamination. In a two-step RT-PCR, synthesis of cDNA is first needed, which is then transferred to a second reaction tube for a subsequent standard PCR. This separation allows for the use of non-specific primers such as random hexamers and/or oligo-dT primers allowing for a multiple gene analysis. A one-step RT-PCR is capable of yielding a higher detection ratio thanks to its intrinsic specificity (De Paula et al., 2004; Drosten et al., 2002; Wacker and Godard, 2005).

1.5. Objectives of this thesis

The main objective of this work is to characterize the viral infection dynamics of HAZV in tick-cell lines along time. The secondary objectives are divided onto three categories:

1. Establish a HAZV culture in mammalian cell lines and determine the proper viral infection parameters to produce a viral stock.
2. Development of a RT-qPCR technique for HAZV viral genomic detection and quantification.
3. Establish tick cell line cultures (HLE/LULS42, HAE/CTVM9 and ISE6) and verify their susceptibility to HAZV infection.
4. Characterize the HAZV infection in tick cell lines and identify the optimal tick cell lines and suitable MOIs for future experiments with HAZV and CCHFV.

2. Materials and Methods

2.1. Design and optimization of a new molecular method for detection and quantification of HAZV genomic material.

Regarding the intent to evaluate the dynamics of infection of HAZV in mammal and tick cell lines along time, a novel TaqMan® based RT-qPCR assay was developed. In this work it was chosen to opt by an absolute quantification using a custom standard, a synthetic oligonucleotide. The HAZV synthetic DNA gene fragment will allow the absolute viral quantification in future qPCR reactions by elaborating viral DNA standard curves. All experiments were conducted on a CFX Connect Real-Time PCR Detection System from Bio Rad® (Bio-Rad, CA, USA). The data generated from each RT-qPCR was analysed with Bio Rad CFX Maestro Software

2.2. Primers & probe construction.

The set of primers and probe used in this project were designed using Primer3® (available online at https://primer3.ut.ee/) for the complete S segment of the HAZV genome (isolate JC280), retrieved from GenBank® (http://www.ncbi.nlm.nih.gov/genbank/). The parameters used on the design of the primers were as follows: minimal length of 18 nucleotides and a maximum length of 24 nucleotides; the Guanine-Cytosine ration between 40% and 55% and a melting temperature (TM) ranging from 56ºC to 65ºC. The probe design criteria were as follows: minimal length of 20 nucleotides and a maximum length of 30 nucleotides and the Guanine-Cytosine ration between 35% and 65%. The probe orientation was also set to Sense regarding the target sequence. The desirable amplicon was also projected to have a desirable size between 80-140 base pairs: Guanine-Cytosine ration between 20% and 80% and a TM varying from 70ºC to 95ºC. Both primers and probe were synthesized by STAB VIDA® (Portugal) and were delivered lyophilised. Upon reception they were resuspend in diethylpyrocarbonate (DEPC)-treated water to a stock concentration of 100µM, and later working aliquots consisting of 10µM were made

using also DEPC-treated water. (This work was performed within a Class II Biological Safety Cabinet (BSC)).

Table 1: Sequences of the pair of primer and probe developed in this work. The probe possesses, at the 5´- end extremity the fluorophore fluorescein (FAM), and at the 3´- end extremity a Black Hole Quencher™ (BHQ1).

Primers	Sequence 5' to 3'
Forward Primer	5' - TGCCGAAATTCCTCAGCTCGAC -3'
Reverse Primer	5'- TGCACACTCCATGATAGGAGCAC -3'
Probe	**Sequence 5' to 3'**
Probe	5' – FAM-AGGGACGCCATCTACAGCTCAGCACTCA-BHQ1 -3'

2.3. Optimization

2.3.1. Primer's concentration

The first step was to evaluate the optimal concentration of the new primer set used to amplify the HAZV synthetic DNA in a qPCR assay. For this, we evaluated different primer concentrations using SYBR green as the fluorophore for qPCR reactions. For this, five different primers concentrations of 100 nM, 200 nM, 300 nM, 400 nM and 600 nM were tested. In addition, the ideal annealing temperature for this reaction was also tested using the five different primers concentrations (above mentioned) together with different annealing temperatures: 54ºC 56ºC and 60ºC. The assays consisted of 10 µL final volume reaction with 5 µL corresponding to the master mix iTaq Universal SYBR® Green Supermix from Bio Rad® (Bio-Rad, CA, USA), 1 µL of a synthetic oligonucleotide (serving as a positive control), a varying volume of the pair of primers in each reaction and DEPC-treated water to some up to the final volume.

2.3.2. Probe concentration

In order to optimize the probe concentration five different concentrations of 50 nM, 100 nM, 150 nM, 200 nM and 250 nM were tested against two constant primers concentrations of 250 nM and 400 nM. These reactions occurred in a 10 µL final volume reaction with 5 µL corresponding to the master mix iTaq Universal Probes® One-Step Supermix from Bio Rad® (Bio-Rad, CA, USA), 1 µL of synthetic oligonucleotides (serving as a positive control),0.25 µL or 0.4 µL of primer and a varying volume of probe in each reaction and an accordingly volume of DEPC-treated water to sum up the final volume of reaction to 10 µL.

2.4. Development of a gBlocks®

To access the kinetics of infection a standard curve, generated by the RT-qPCR assays, is necessary to properly quantify the HAZV viral genomic material. With that in mind, a valid standard template is necessary. For that purpose, a custom standard was idealized using a synthetic oligonucleotide such as gBlocks®, Gene Fragments, from Integrated DNA Technologies (IDT, IA, USA), which has proven to be an accurate and quick solution when developing a custom standard in a probe-based qPCR (Conte et al., 2018). Similar studies focussing on quantifying other viruses, also using RT-qPCR, used gBlocks® (Marthaler et al., 2014) or other type of synthetic oligonucleotides, and revealed that the synthetic base standard curve displays the same ability to quantification and thus can be a valid replacement for conventional standard curves (Bandeira et al., 2020)The design of the custom standard was made manually by analysing the S segment of the HAZV genome (isolate JC280), retrieved from GenBank® and encompassing previously outlined regions of the HAZV genome defined by the set of primers used in this work and also of two other set of primers described in literature (Lewandowski et al., 2017; Matsumoto et al., 2018). The gBlocks® had a length of 496 nucleotides (Figure 7) with a GC content of 45,77%. After receiving the dried gBlocks®, it was resuspended in DEPC-treated water according to the manufacturer's instructions. In all subsequent qPCR assays this gBlocks® was used not only as a template to the standard curves by performing serial dilutions, but also as a positive control.

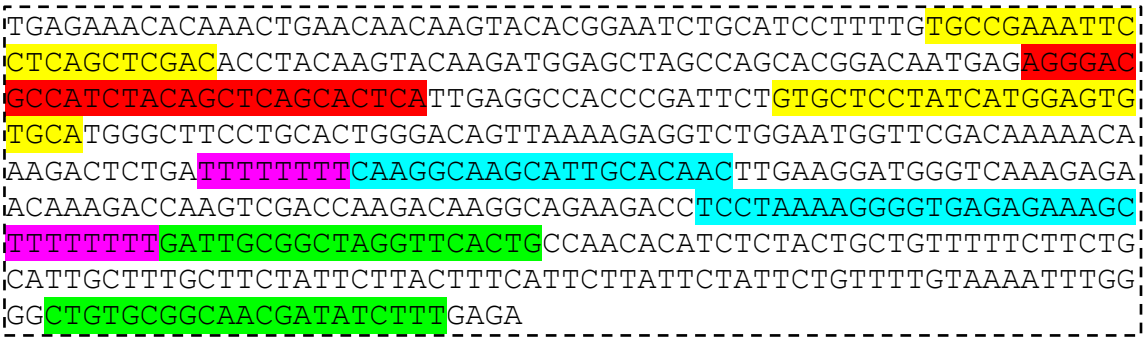

Figure 7. DNA sequence of the gBlocks®. The regions of the HAZV genome defined by this thesis set of primers are highlighted in yellow, and the probe highlighted in red. Two other literature described set of primers from Lewandowski et al., 2017 in blue and from Matsumoto et al., 2018 in green. The repetition of eight thymine (in purple) indicates the position of linkers, used to connect different DNA sequences.

2.5. Cell lines

2.5.1. Mammalian cell lines

Four different types of mammalian cell lines were used throughout this study in several experimental procedures. Vero E6 cells (ATCC CRL-1586™), derived from kidney of African green monkey (*Cercopithecus aethiops*), A549 cells (ATCC CCL-185™), derived from the human alveolar basal epithelium and Caco-2 cells (ATCC HTB-37™), derived from human colon adenocarcinoma cell line, were all obtained from the cell lines collection at Institudo de Higiene e Medicina Tropical (IHMT). SW13 cells (ATCC CCL-105™), derived from a human adrenal cortex carcinoma line were kindly provided by Dr. Cristiano Salata from Università degli Studi di Padova.

2.5.2.Maintenance and growth of mammalian cell lines.

Vero E6, A549 and Caco-2 cell lines were cultured in Dulbecco's Modified Eagle Medium (DMEM) (Biochrom Dulbecco´s MEM) (Biochrom, Berlin, Germany) supplemented with 10% Fetal Bovine Serum (FBS), heat inactivated, (Gibco™) (Life

Technologies, Carslsbad, USA) and Pen/Strep 10,000 U/mL Penicillin and 10,000 µg/mL Streptomycin (Gibco™). Caco-2 cell line medium was also supplemented with 1% non-essential amino acids (NEAA) 100X (Biowest®). SW-13 cells were cultured using Leibovitz's L-15 Medium (Gibco™) supplemented with 10% FBS (Gibco™) and 2nM of L-glutamine 200X (Gibco™). All cell lines were growth in flasks and incubated at a temperature of 37º with 5% CO2 in a humidified incubator (Sanyo MCO-18AIC-UV-CO2 Incubator), except for the SW-13 cells which were maintained at 37ºC in a humidified incubator. The cell lines were passaged when it´s growth would reach almost confluency (every 3-4 days) using Trypsin-EDTA 0.25% (Biochrom).

2.5.3. Tick cell lines

Ixodes scapularis ISE6, *Hyalomma anatolicum* HAE/CTVM9 and *Hyalomma lusitanicum* HLE/LULS42 cell lines were acquired from the Tick Cell Biobank (https://www.liverpool.ac.uk/health-and-life-sciences/research/liverpool-shared-research-facilities/bio-resources/tick-cell-biobank/) through a collaboration with Dr Lesley Bell-Sakyi from the University of Liverpool.

2.5.4. Maintenance and growth of tick cell lines

ISE6 cells were cultured in L15B300 medium (3 parts L15B to 1 part H_2O Milli-Q) supplemented with 10% FBS, 0,1% Lipoprotein, 2 mM L-glutamine and Pen/Strep 10,000 U/mL Penicillin; 10,000 µg/mL Streptomycin. HAE/CTVM9 cells were cultured in L15/MEM with Hank´s salts medium (1 part L15 to 1 part MEM with Hank´s salts) and supplemented with 10% Tryptose Phosphate Broth 1X (TPB), 20% FBS, 2 mM L-glutamine and Pen/Strep 10,000 U/mL Penicillin; 10,000 µg/mL Streptomycin. HLE/LULS42 cells were cultured in L15/L15B medium (1 part L15 to 1 part L15B) and supplemented with 10% Tryptose Phosphate Broth (TPB), 20% FBS, 2 mM L-glutamine and Pen/Strep 10,000 U/mL Penicillin; 10,000 µg/mL Streptomycin. All mentioned reagents were from Gibco™. Tick cell lines were maintained in sealed 2mL Nunc™ tubes (in some cases ISE6 were also cultured in T-25cm flasks) and incubated at 32ºC in *Heraeus* Heracell 240 CO^2 Incubator (without CO_2)

2.6. Hazara virus

The HAZV stock was kindly provided by Dr. Babak Afrough from the Public Health England (PHE) through the European Virus Archive (Ref-SKU: 005v-EVA635). The HAZV stock, previously titred using TCID50 at 6.3 x 10^6 per mL (equivalent to 4×10^6 plaque forming units (PFU) per mL) was used to perform Multiplicity of Infection (MOI) assays to determine the optimal ratio between virus and the different cells used, to find the optimal conditions for virus cultivation. All work was conducted in an appropriate MSC II geared to virus work whenever handling HAZV.

2.6.1. Multiplicity of Infection assay

Before advancing to HAZV production, it was first necessary to establish infection parameters in order to achieve an optimal viral production to generate a HAZV stock for future uses. Thus, a series of MOI assays was performed. Vero E6 cells were chosen to be infected with HAZV for stock production as these cells were already available in the IHMT collection (likewise they were already adopted in various IHMT studies whereas a viral production was necessary).

Vero E6, A549, Caco-2 and SW-13 cells were grown in their respective medium and were used to seed 12-well plates. When the cells achieved 70-80% confluency they were infected with HAZV stock in serum-free DMEM (SF-DMEM), or with SF-L15 for plates containing SW-13 cells, (previously prepared based on the cell count at confluency and the titre of HAZV) as such: 300 µL of virus were added into the side of each well, accordingly to the respectively MOI, and the plates were left to incubate, allowing the virus to adsorb to the cells, for 1 hour at 37ºC and 5% CO2. After one hour of incubation the medium with the virus was retrieved. The plates seeded with Vero E6, A549 and Caco-2 had each well supplemented 1 mL of DMEM containing 2% FBS (and 1% NEAA for Caco-2 cells), as for the plates seeded with SW-13 each well was supplemented with 1 mL of L15 containing 2% FBS. All plates were placed at 37ºC, 5% CO2 in humidified incubators. Following 24, 48, 72 and 96 hours after infection the wells were examined for any evidence of cytopathic effect (CPE) and the supernatant was collected and clarified by centrifugation at 3000 x g for 5 minutes at 4 °C and later

stored in a microcentrifuge tube and kept at -80°C until further processing. In some cases, in the interest of recovering any intracellular forms of the virus, the plates underwent a process of freeze-thawing the adherent cells at -80ºC for 15-20 min followed by retrieving the supernatant and handling as previous described.

2.6.2. Hazara virus growth and cultivation

HAZV at 4×10^6 pfu/ml was inoculated into flasks with Vero E6 at a MOI of 0.01. After one hour of incubation the virus was retrieved and the flasks were supplemented with DMEM with 2% FBS and incubated for 96 hours at 37ºC, 5% CO2. After four days, the virus was harvested and quantified using RT- qPCR rendering a viral concentration of 9×10^7 genomic equivalents per mL. This stock of HAZV was then used in all subsequent procedures. In addition, this viral stock was also quantified via plaque assay using SW-13 cells, to quantify infectious plaque-forming units (PFU) in the produced viral stock to obtain the viral titre of the effective virions.

2.6.3. HAZV plaque assay using carboxymethyl-cellulose

SW-13 cells were seeded in 12-well plates with L15 containing 10% FBS medium and when they reached confluency, the medium was recollected. After, HAZV virus was added in triplicates (previously diluted in 10-fold serial dilutions in SF-L15), incubated for one hour at 37º, followed by an overlay consisting of one-part 2% Carboxymethylcellulose (CMC) (CMC sodium salt, low viscosity Merck) to one-part L15 2X supplemented with 5% FBS (in some instances an overlay of 3% CMC was used). The plates were incubated for 6 days at 37º without agitation. Cells were fixed by adding 20% formaldehyde in phosphate buffered saline (PBS) (Sigma-Aldrich®) (Sigma-Aldrich, St. Louis, MO, USA) per well for one hour. To remove formaldehyde, the plates were submerged in water and washed once. A solution of crystal violet was used to cover the surface of each well for 15-20 minutes before the removal of the dye by submerging the plates in water and washing the wells. The plaques were then counted (whenever CPE was present) resulting in a viral titre of $9{,}3\times10^5$ pfu/mL for CMC 2% and $3{,}0\times10^5$ pfu/mL for CMC 3%, calculated following the given formula (Figure 8).

$$PFU/mL = \frac{Average\ number\ of\ plaques}{Dilution \times Inoculum}$$

Figure 8: Viral titer equation (PFU/mL). Dilution represents the dilution in which the plaques where counted and inoculum refers to the volume of inoculum in mL of diluted virus added to the plate.

The same protocol was also applied to Vero E6 cells (using it´s corresponding medium and having an incubation with 5% CO_2) However, it was not possible to observe plaques in any assay using Vero E6 cells infected with HAZV.

2.6.4. HAZV plaque assay using agarose

Agarose was also tested as an overlay media to compare with CMC results. For this, SW-13 cells were seeded in 6-well plates with L15 containing 10% FBS medium. When confluency was obtained, the medium was collected and HAZV virus was then added in triplicates (previously diluted in 10-fold serial dilutions in SF-L15) incubated one hour at 37ºC, followed by an overlay media, consisting of diluting one-part 2% agarose (ultrapure grade from Nzytech, Lisboa, Portugal) to one-part L15 2X supplemented with 5% FBS. The plates were incubated for 4-6 days at 37º without agitation. Cells were fixed by adding 20% formaldehyde (in PBS) per well for one hour. To remove formaldehyde, the plates were submerged in water and washed once. A solution of crystal violet was used to cover the surface of each well for 15-20 minutes before the removal of the dye by submerging the plates in water and washing the wells. The plaques were then counted (whenever CPE was present), using the formula expressed in Figure 8, resulting in a viral titre of $3{,}6\times10^6$ pfu/mL.

2.7. Tick cell lines infection

ISE6, HAE/CTVM9 and HLE/LULS42 cells were seeded at a density of 5×10^5 cells per mL in sealed flat sided culture tubes (Nunc™ tubes) and cultured with 2mL of their respective cell culture medium and incubated at 32º without CO_2. After two days, culture medium was removed, and cells were infected with one mL of HAZV at the

appropriate MOI (0.1, 1 or 5) in complete medium for one hour at 37ºC. All infections were performed in triplicates. A blank tube sample (for each of the different cell lines) was treated with complete medium without virus, serving as a negative control throughout the experiment. The medium containing HAZV was then carefully totally removed and new complete medium (2 mL) was added to each tube. The cultures stayed in incubation at 32ºC without CO_2 until the end of the experiment.

2.7.1. Hazara virus infection kinetics in tick cell lines

To evaluate the HAZV infection kinetics in each tick cell line, 200 µL of supernatant medium was collected from the cultures at specific time points and an equal volume of fresh medium was replaced in the culture tubes. Supernatants were stored in -80Cº until further processing. RNA extraction was made on 50 µL of the collected supernatant from the various time points for molecular quantification.

2.8. RNA extraction

The viral genetic material was harvested from the supernatant via phase separation using NZYol® (Nzytech, Lisboa, Portugal) according to the manufacturer's instructions. NZYol® was added in a proportion of three to one to each sample and incubated five minutes at room temperature. Chloroform was then added (in a proportion of one part chloroform to five parts NZYol®) and the samples were mixed vigorously for 15-20 seconds. After an incubation period of three minutes at room temperature, samples were submitted to a centrifugation step at 12,000g for 15 minutes at 4ºC. The resulting aqueous phase was transferred to a new tube. To ensure the RNA precipitation, ice-cold isopropyl alcohol was added to the samples (in a proportion of one part isopropyl alcohol to two parts NZYol®) and incubated 10 minutes in -20ºC. Samples were centrifuged at 12,000g for 10 minutes at 4ºC and the supernatant was discarded. The RNA pellet was washed using ice-cold 75% ethanol (in a proportion of one part Ethanol to one part NZYol®) and the samples were once again centrifugate at 12,000g for 10 minutes at 4ºC discarding the ethanol supernatant and ensuring the pellet would dry. The RNA pellet in the samples was finally resuspended in 30 µL of nuclease-free water. RNA samples were kept in -80ºC until further processing. Blank samples were

processed for RNA extraction equally to infected samples, and the final product was also stored at -80ºC.

2.9. Reverse transcription quantitative PCR (RT-qPCR)

The assessment of the genomic material in the samples was conducted via One-Step TaqMan® probe RT-qPCR. All the samples were analysed in duplicates. Every reaction consisted of a 10 µL total volume of which 5 µL were of iTaq Universal Probes One-Step Kit Master Mix from BioRad®, 250 nM of each primer, 50 nM of probe and 3 µL of RNA to be analysed. Nuclease-free water was added to a final reaction volume of 10 µL. The cycling conditions used were as indicated in Table 2, and the fluorescence data was collected after each 60 ºC annealing step. The standard curve was created using as template, 10-fold serial dilutions of gBlocks®. The analysis of the mock-infected samples (the negative infection control) was also conducted and was treated the same way as other samples. A negative reaction control, with DEPC-treated water instead of the RNA template but containing all other components of the reaction mix, was used to test for possible contamination.

Table 2: Cycling conditions of the RT-qPCR assays.

	Temperature	Time	Cycles
Initial denaturation	95ºC	5 min	1
Denaturation	95ºC	10 sec	40
Annealing	60ºC	30 sec	
Extension	72ºC	20 sec	

2.10. Data analysis

Statistical analyses and graphics were made with GraphPad Prism v9.0.0 (121). HAZV Viral copy numbers were compared using the Ordinary one-way Anova multiple comparisons test. P-values greater than 0.05 were considered non-significant.

3. Results

3.1. Optimization of the molecular method to detect and quantify Hazara virus.

3.1.1. Primer optimization using SYBR Green

The optimal temperature of annealing was defined at 56ºC since it enabled the binding of the primers to the complementary region with a high efficacy. Although higher efficacies were obtained at a temperature of 54ºC (as show in Table 3), ultimately, an ideal annealing temperature of 56ºC was chosen, in order to promote higher specificity of binding, together with the addition of an extension step at 60ºC in every reaction.

Table 3. Efficiency and R values obtained in the different assays to determine the optimal annealing temperature and primer concentration for the RT-qPCR assay. A qPCR efficiency is basically a ratio between the number of the amplified target molecules (at the end of a amplification cycle) divided by the number of the same molecules at the beginning of such PCR cycle. The efficacy should range between 90% and 110%. The standard curve generated should encompass the expected range of target concentrations in the samples, hence the R value (correlation coefficient) evaluates how well the generated data matches in the standard curve. Generally, R values > 0.990 are considerate good measures the accuracy of the generated standard curve.

	Annealing temperature							
	54ºC		56ºC (1)		56ºC (2)		60ºC	
Primers [nM]	efficiency	R	efficiency	R	efficiency	R	efficiency	R
100	91,00%	0,980	77,80%	0,998			83,70%	1,0
200	108,80%	0,997	85,90%	0,998	80,80%	0,983	85,40%	0,996
300			76,50%	0,998	92,40%	0,995	90,70%	0,997
400	107,80%	0,998	103,20%	1,0	82,90%	0,993	90,30%	0,998
600	113,90%	0,995						

To achieve the ideal primer and probe concentration in the reaction, the goal was to obtain the lowest concentration of primer and probe which would generate a high efficiency and low quantitation cycle (Cq) values. The Cq values obtained in the five different primers concentrations had no visually apparent differences between them.

3.1.2. Probe optimization.

The probe optimization assays showed no clear difference between the different concentrations used regarding the efficiency of the reaction (Table 4). The lowest Cq value was obtained at a probe concentration of 100 nM in combination with a primer concentration of 250 nM (which was latter applied in all subsequent reactions).

Table 4. Efficiency and R values calculated for several probes concentrations.

	Primer [250nM]		**Primer [400nM]**	
Probe [ ] nM	efficiency	R	efficiency	R
50	82,30%	0,986	71,00%	0,993
100	78,00%	0,997	83,50%	0,996
150	81,20%	0,992	76,40%	1,0
200	74,00%	0,996	81,30%	1,0
250	82,70%	0,991	94,30%	0,979

3.2. HAZV infection on mammalian cell lines

3.2.1. Multiplicity of infection assays

In the first MOI assay, infections of Vero E6 cells were carried out at an MOI of 0.1; 0.01 and 0.001 and supernatant samples for viral quantification were collected at four distinct moments (1dpi, 2dpi, 3pi and 4dpi). Despite susceptible to infection and producing viral copies of HAZV detectable by RT-qPCR, Vero E6 cells did not show any evidence of cytopathic effect (CPE) (Figure 9). Howbeit this first assay proved that

Vero E6 cell were suitable for HAZV infection, unfortunately the negative controls were contaminated. Therefore, a new assay was carried out similarly to the previous one except that the tested MOI were only of 0,1 and 0,01. Upon recollection of supernatant samples (1dpi, 2dpi, 3dpi and 4dpi), the RNA was extracted and quantified trough RT-qPCR. The viral titre obtained is showed in Figure 10. Statistical analysis revealed no significant difference between the various time points and MOI used. Therefore, it was chosen to carry out the infection in Vero E6 cell using a MOI of 0.01 and extracting the supernatant for viral harvest after 4 days since infection. This decision was made to produce a significant quantity of HAZV as a stock for future studies and for use in this work.

A549 cells and Caco-2 cells were also used in a MOI assay. However, the finality of this experiment was to learn if these two cell lines (also available at IHMT) were suitable for infection and, more importantly, if showed evidence of CPE formation, hence if were capable of being used in plaque assays. Unfortunately, A549 and Caco-2 cell lines revealed no evidence of CPE, thus being discarded for future use.

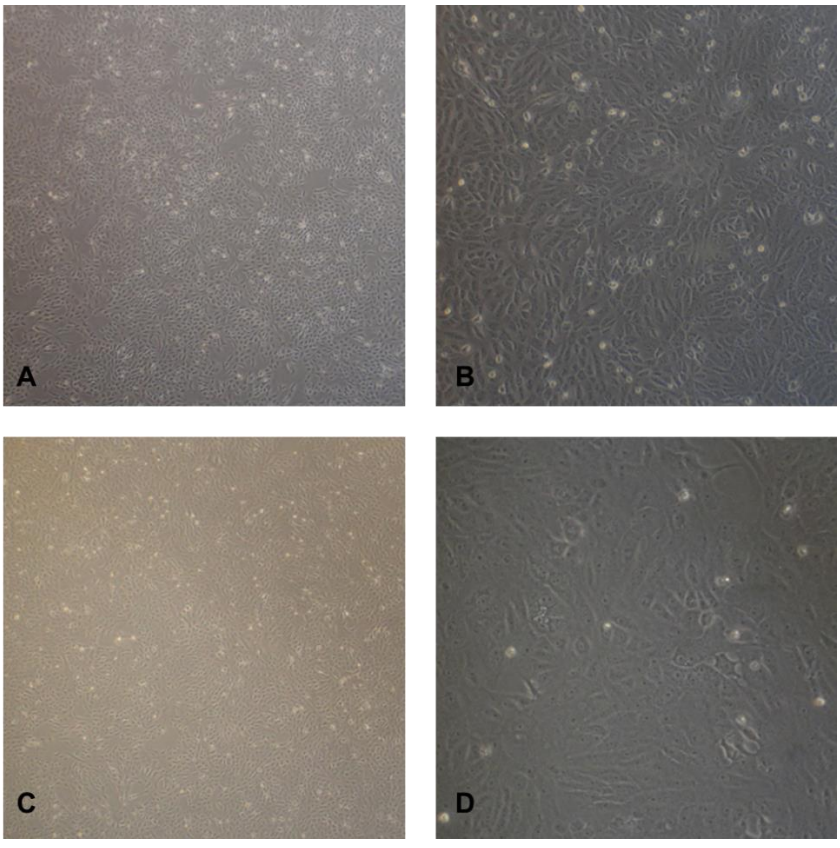

Figure 9. Morphology of Vero E6 cells. Vero E6 cells during normal growth phase (A and B) and photos of Vero E6 taken 48h pi at a MOI of 0.01(C and D). Notice no visible sign of cytopathic effect in pictures C and D.

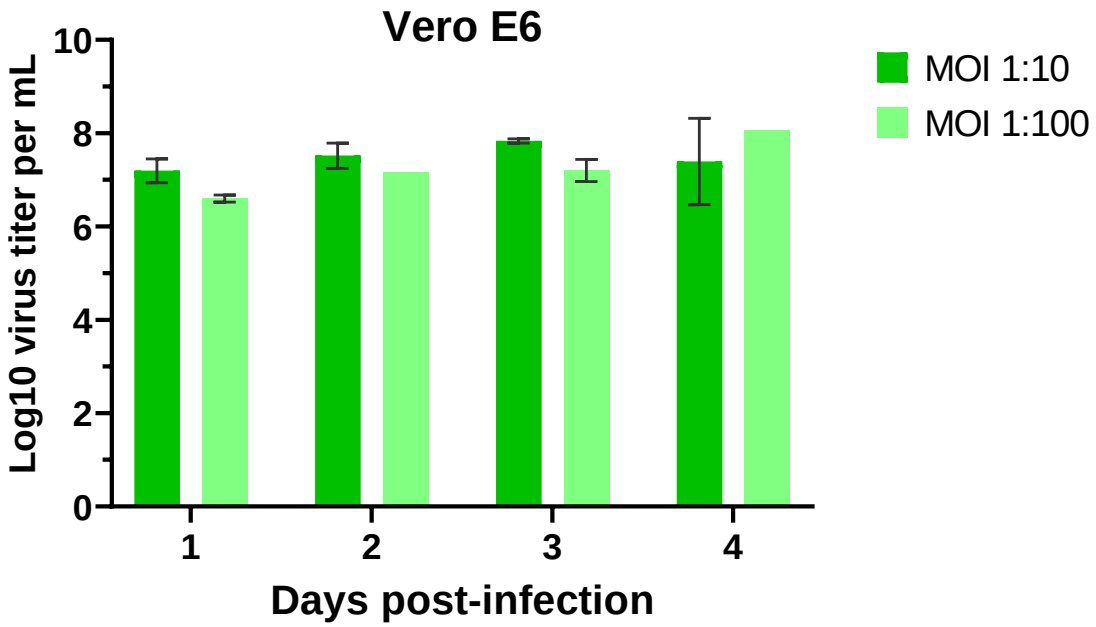

Figure 10. HAZV viral titres obtained in Vero E6 infected cells. Mean values of virus per mL (in log10) calculated for each dpi in Vero E6 cells infected with HAZV. (The error bars represent standard deviation ((S.D.)). Although a slight increase of viral copies is found in Vero E6 cells infected at an MOI of 0.1, statistical analysis showed that no significant differences to the viral titre obtained by cell infected with MOI of 0.01.

SW-13 cells, later provided by Dr. Cristiano Salata, were requested to be used as template for viral plaque assays, as SW-13 cells are the only cell lines capable of producing visible plaques in viral plaque assays. This information was not available in the scientific literature and even the EVAg virus supplier did not provide this valuable information on time. Upon arrival, it was decided to perform the same MOI assays on SW-13 cells using the same protocols used for the previous cell lines stated above.

SW-13 cells were infected at a MOI of 0.1, 0.01 and 0.001 and had the supernatant collected at 1 dpi, 2 dpi, 3 dpi and 4 dpi. As suggested in the protocol sent from the virus supplier (Dr. Babak Afrough), it was decided to recover any intracellular forms of the virus by freeze-thawing the adherent cells at -80'C for 30 min at 2 dpi and 4 dpi. In contrast with Vero E6 cells, SW-13 cells, that are widely used as a template for viral production and plaque assays when working with hemorrhagic viruses (Földes et al., 2020b), displayed signs of cytopathic effect clearly visible at 48 hours pi (Figure 11). Posterior quantification and analysis of the results (Figure 12) showed significant

differences between the viral titre achieved by each MOI in the first 3 dpi and a visible difference between the MOI of 0.1 compared to the other two. Despite this trend, there is no significant difference between the viral titre values between 3 dpi and 4 dpi. Also note that the viral titre values obtained for the sample that underwent freeze-thawing process 2 dpi are clearly higher when compared with the values collected from the same day. When comparing viral titres at 4 dpi between samples not submitted to freeze-thawing and those submitted, no significant difference is observed ($p > 0.05$)

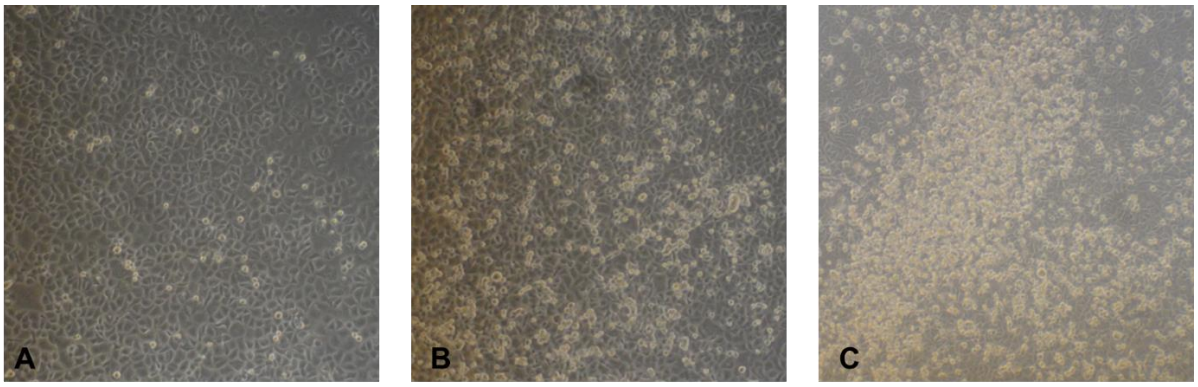

Figure 11. Morphology of SW-13 cells. SW-13 cells during normal growth phase (A). Pictures SW-13 cells taken after infection with HAZV at a MOI of 0.01 (B- 48 hours pi; C 72 hours pi).

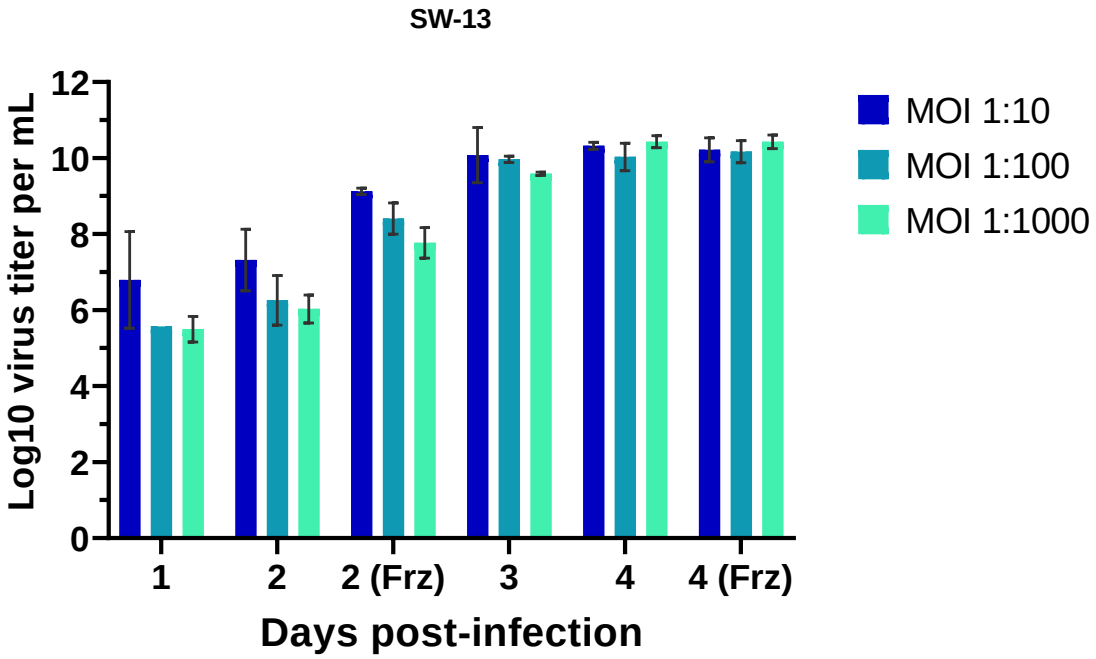

Figure 12. HAZV viral titres obtained in SW-13 infected cells. Mean values of virus per mL (in log10) calculated for each dpi in SW-13 cells infected with HAZV (error bars represent S.D.). Frz represents the samples in which a freeze-thawing process was applied (2dpi and 4dpi).

3.2.2. HAZV stock production and quantification

Vero E6 cells were infected with HAZV at an MOI of 0.01 and after 96 hours the supernatant was recollected and underwent RNA extraction. Extracted RNA samples were quantified via One-Step TaqMan® probe RT-qPCR. Results are showed in Figure 13. Calculation of the number of viral copies showed an average of $2{,}90\times10^{6}$ copy number which translates into $9{,}60\times10^{7}$ genomic equivalents per mL.

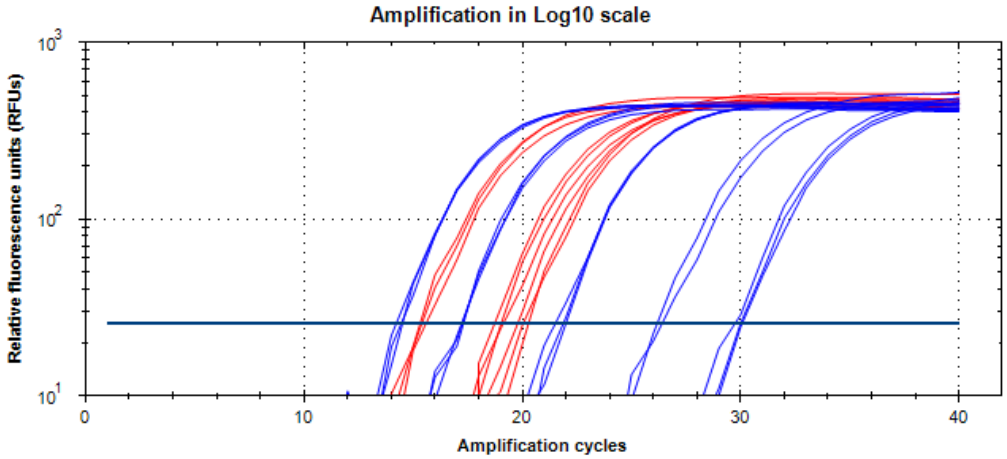

Figure 13. Amplification graph of the RNA samples quantified from HAZV production on Vero E6 cells. Blue lines represent the standard curve (efficiency of 77%) and the red ones correspond to the RNA samples analysed.

3.2.3. Viral titration using plaque assays

Before infecting tick-derived cell lines with HAZV, it was necessary not only to quantify molecularly the viral stock produced, but also to determine the effective viral titre using plaque assay. The latter was performed using Vero E6 cells. However, as previously stated, this cell line does not form any visible CPE (Figure 9), ensuing that no visible plaques were observable in any assay realized (Figure 14).

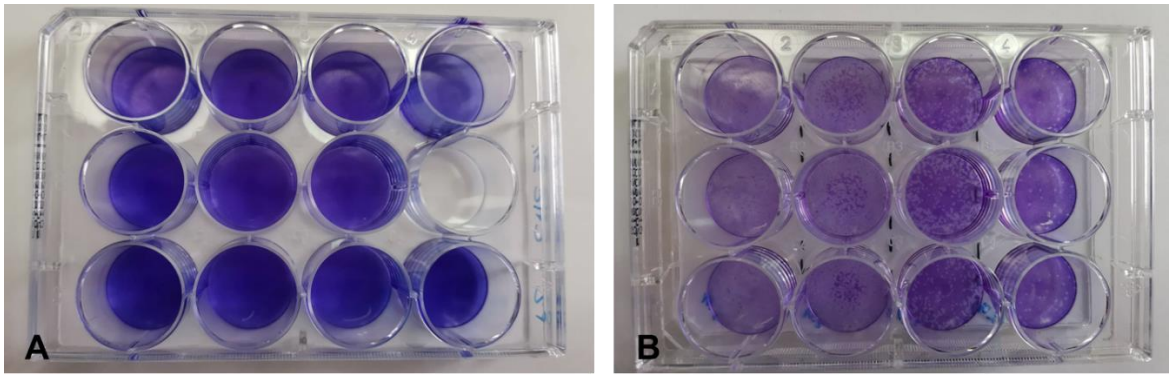

Figure 14. Viral plaque assay. Plaques assay using Vero E6 cells (A) in which each well has a uniform monolayer of cells versus plaque assay using SW-13 cells (B) displaying formation of viral plaques (Both assays were performed using the same overlay, CMC 2%, incubated 6 days prior to fixation and staining).

After several efforts to quantify the HAZV production with Vero E6 cells, Dr. Cristiano Salata provided SW-13 cells which enable to properly conduct a plaque assay using these cells. Plaque assays using SW-13 revealed to be successful at quantifying the virus. The two-overlay media used (CMC or agarose) displayed slight differences (Figure 15) on the number and size/morphology of plaques that were counted and expressed in PFU/mL. The plaques where CMC at 2% was used as overlay medium resulted in a viral titre of $9{,}3\times10^5$ pfu/mL and $3{,}0\times10^5$ pfu/mL for CMC 3%, while the use of agarose resulted in plaques rendering a viral titre of $3{,}6\times10^6$ PFU/mL.

A contrast is present when comparing the PFU results from plaque assay with the viral genome counts from the molecular viral quantification process which was generally more than 1 order of log10 scale higher than the PFU particle counts.

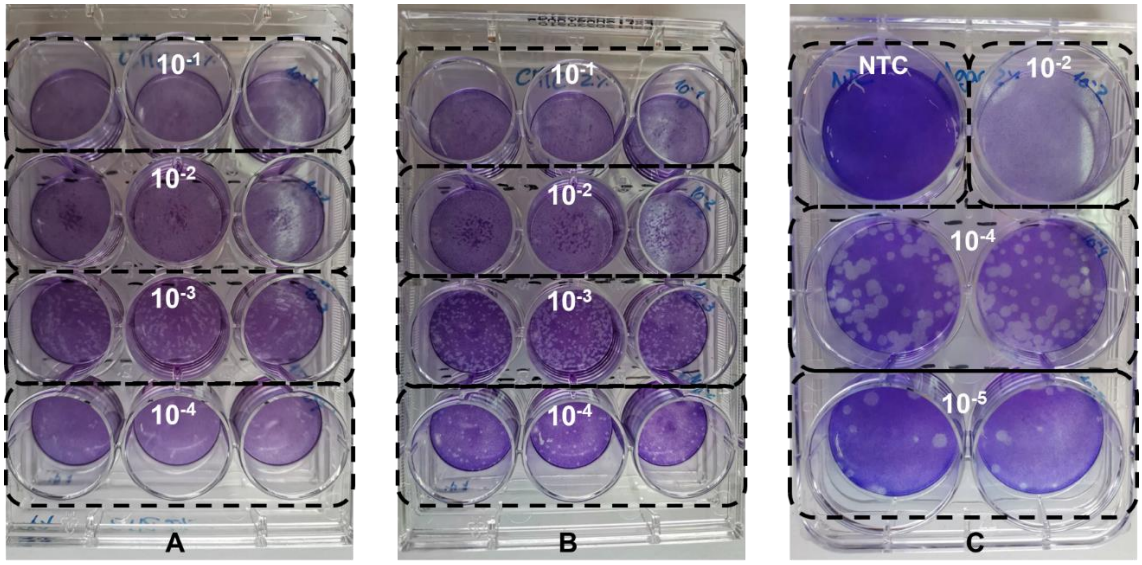

Figure 15. Plaque overlay comparison. SW-13 cell were plated and later infected with serial dilutions (expressed in white) of HAZV. An overlay of CMC 2% or 3% was applied (A and B correspondently) and a separate experiment used Agarose 2% as overlay (C). Viral plaques were visually counted on wells having no fewer than 10 or greater than 100 plaques (for the plates using CMC this usually happens in a lower dilution compared with agarose). The blank control (NTC) displays a uniform cell monolayer.

3.3. Tick cell lines infection with HAZV

To evaluate the kinetics, effects of infection and viral replication in tick-derived cell lines, HLE/LULS42, HAE/CTVM9 and ISE6 cells were infected with HAZV. As expected, neither of the cell lines displayed any visible sign of CPE (Figure 16), nor any visible changes were observed on the cells medium that would point out to any kind of cellular stress. Following infection, the three different tick-derived cell lines had their supernatant recollected at specific time points. After extraction and posterior quantification by RT-qPCR the viral genomic material present in the sample was analysed to evaluate the kinetics of infection along time.

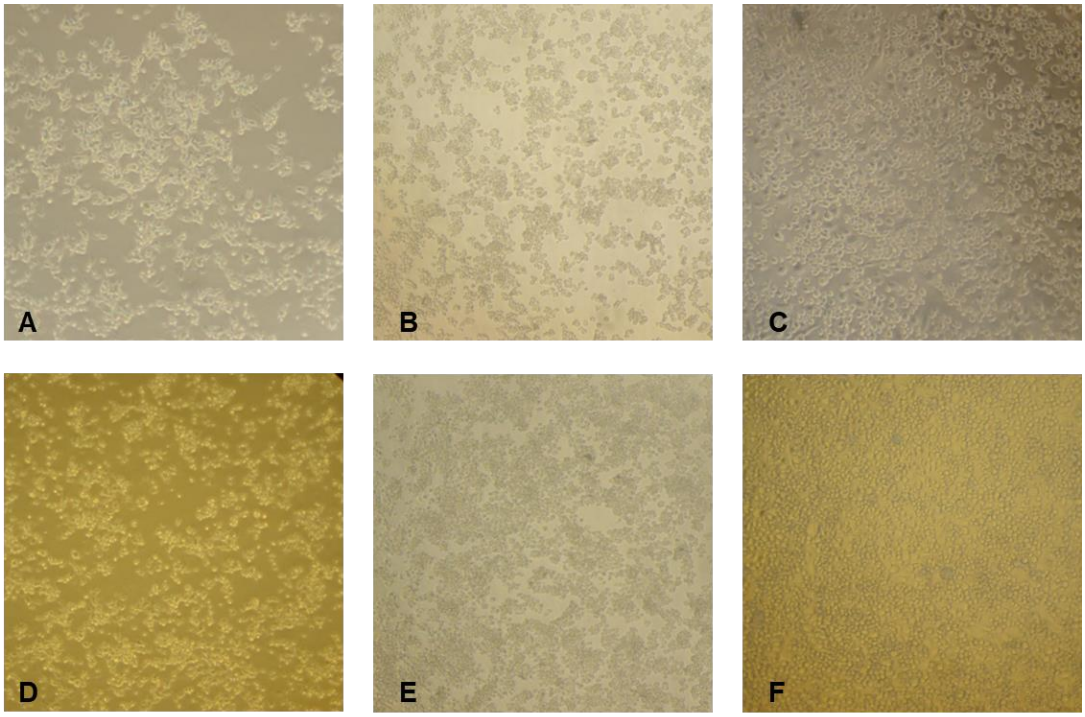

Figure 16. Morphology of HLE/LULS42 (A); HAE/CTVM9 (B) and ISE6 (C) cell lines taken during normal cell cycle in the first row. After infection with HAZV (second row) the cells displayed no sign of cytopathic effect (D- HLE/LULS42; E- HAE/CTVM9; F- ISE6).

3.3.1. *H. lusitanicum* – HLE/LULS42

To study the progression of infection in the first stages of infection and how it would relate to the viral capacity to replicate in the first days after infection, supernatant samples were collected everyday up to the tenth day post infection on HLE/LULS42 cells. The quantification of viral genomic material on those ten first days are showed in Figure 17. The mock-infected HLE/LULS42 cells did not tested positive for HAZV detection in any of the RT-qPCRs performed (data not showed).

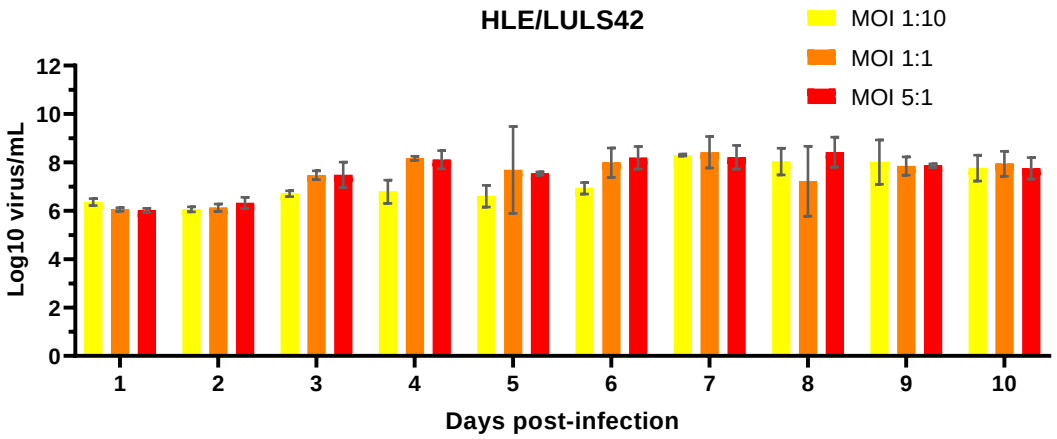

Figure 17. HAZV infection of *H. lusitanicum* cells. Mean values of virus per mL (in log10) calculated in the first 10 consecutive days post infection of the HLE/LULS42 cell line with HAZV . The different MOIs used are represented by distinct colour. The evaluation of the increase of viral RNA was made by RT-qPCR analysis. (The error bars represent S.D.).

The results suggest a peak in concentration of genomic material in achieved around the 7 or 8 dpi, followed by a stabilization of the values, showing a formation of a persistent infection. Statistical analysis performing multiple comparisons between samples showed that despite the three different MOIs used in the infections, there was no significant differences between virus per mL values between MOIs at each respective dpi. However, the same analysis exposed a difference on the kinetics of viral progeny release in which, for all the three MOI used the first two time points of analyse showed a significant pairwise comparison (below established threshold of 0.05) to both the 7 or 8 dpi, furthermore hinting at a peak of viral production at those

days after infection. Additional analysis revealed that the values of viral genomic material found in HLE/LULS42 cells maintain their levels stabilized during the duration of this experiment, as showed in Figure 18, suggesting the capacity of this cell line to maintain a detectable viral load even after 80 dpi.

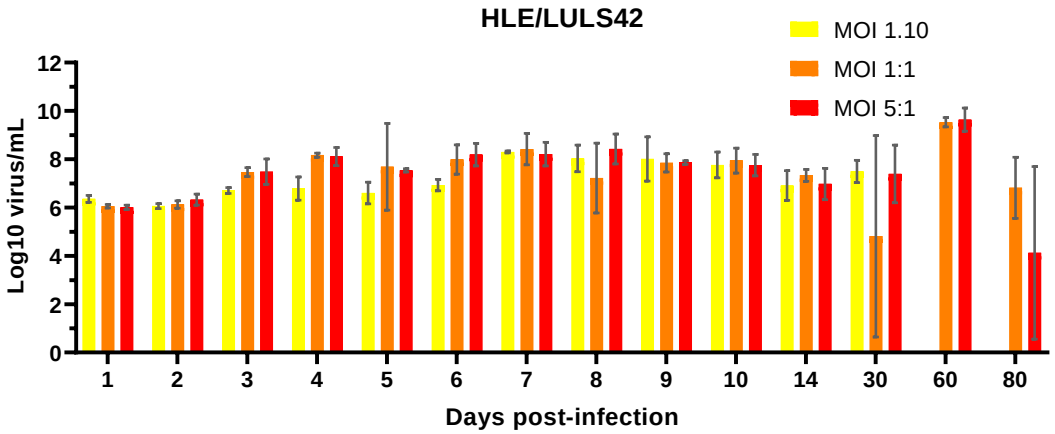

Figure 18. HAZV infection of H. lusitanicum cells throughout the duration of experiment. Mean values of virus per mL (in log10) calculated throughout this work for the HLE/LULS42 cell line. The different MOIs used are represented by distinct colour. The evaluation of the increase of viral RNA was made by RT-qPCR analysis. Note that the last two values for the MOI of 1:10 do not appear as the samples associated with these values were not collected due to fungi contamination. (The error bars represent S.D.).

3.3.2. *H. anatolicum* – HAE/CTVM9

Relatively to *H. anatolicum* – cell line the main purpose was to observe, and compare with the others cell lines, their behaviour and evolution after infection. As this cell line was recently the object of a major study regarding persistent infection by HAZV (Salvati et al., 2021), it was decided not to collect samples from consecutive days post-infection but to analyse the evolution of the infection and compare the results with those obtained for the other cell lines. As such, Figure 19 demonstrates a clear formation of a persistent infection with viral loads detectable throughout the course of this work. Statistical analysis revealed no significant difference between the yield of virus per mL between the three different MOI used in the experiment for each day-post infection. The mock-infected HLE/LULS42 cells did not tested positive for HAZV detection in any of the RT-qPCRs performed (data not showed).

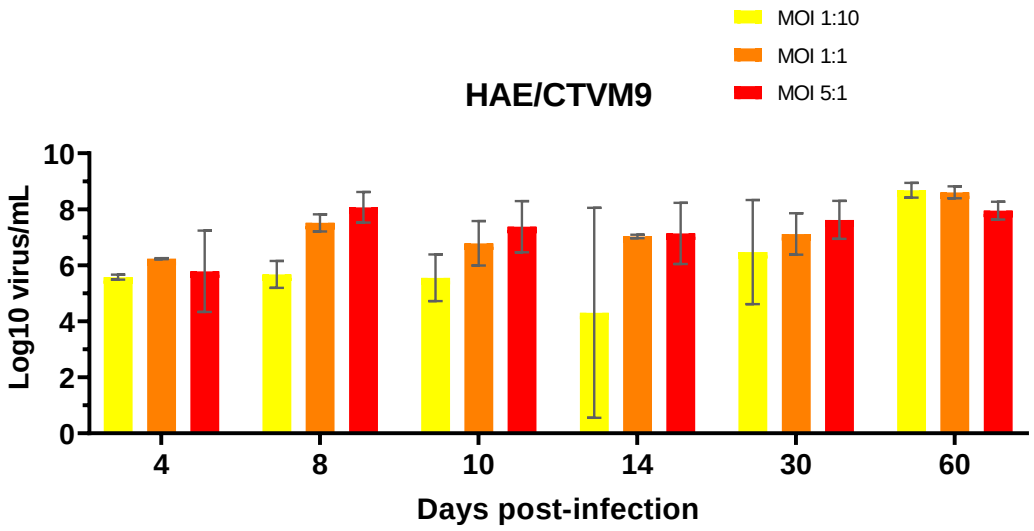

Figure 19. HAZV infection of *H. anatolicum* cells. Mean values of virus per mL (in log10) calculated throughout this work for the HAE/CTVM9 cell line. The evaluation of the increase of viral RNA was made by RT-qPCR analysis. The different MOIs used are represented by distinct colour. No significant difference was found on the yielding of viral titre by the three different MOIs. (The error bars represent S.D.).

3.3.3. *I. scapularis* – ISE6

Analysis of the RNA samples collected and quantified revealed that the values of viral genomic material found in ISE6 cells stabilizes during infection. The mock-infected HLE/LULS42 cells did not tested positive for HAZV detection in any of the RT-qPCRs performed (data not showed). Statistical analysis demonstrated no significant difference between the yield of virus per mL between the three different MOI used in the experiment during the onset of infection, albeit the last two time points (see Figure 20) in which each point referencing to an infection MOI of 0,1 had showed a significant pairwise comparison (bellow established threshold of 0.05) to each of the two samples collected in the same day.

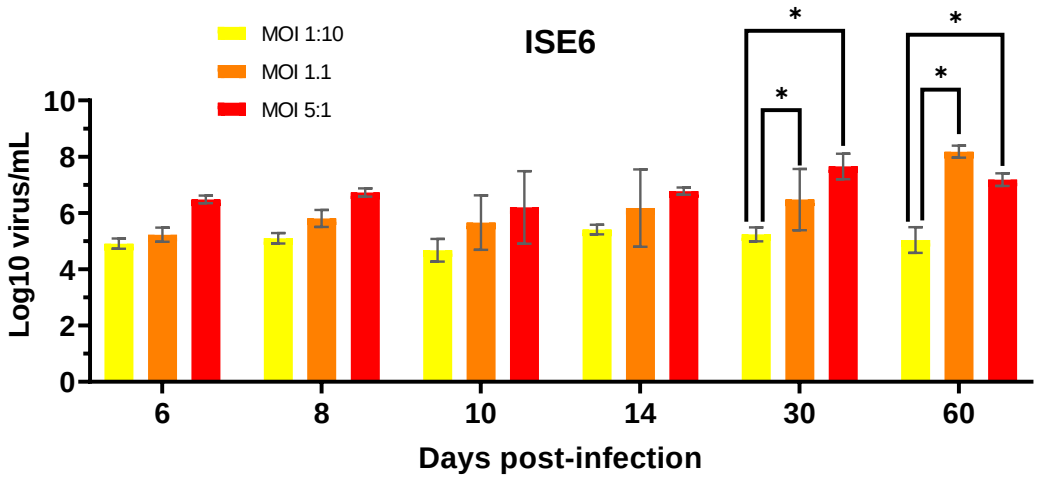

Figure 20. HAZV infection of *I. scapularis* cells. Mean values of virus per mL (in log10) calculated throughout this work for the ISE6 cell line. The evaluation of the increase of viral RNA was made by RT-qPCR analysis. The different MOIs used are represented by distinct colour. Significant results ($p < 0.05$) are showed in the graph with a *. (The error bars represent S.D.).

3.4. Comparison of HAZV infection levels in tick cell lines

Analysing the results of HAZV replication in each different cell line revealed not only a relative increase in viral RNA with a peak around the 8 dpi (as previously stated) but also point out to a clear preference of host cell for this virus. Results suggest that the kinetics of replication of HAZV in HLE/LULS42 are higher when compared with the other two tick cell lines. Furthermore, this robust production of HAZV viral particles by HLE/LULS42 is independent on the different MOI used for infection (Figure 21).

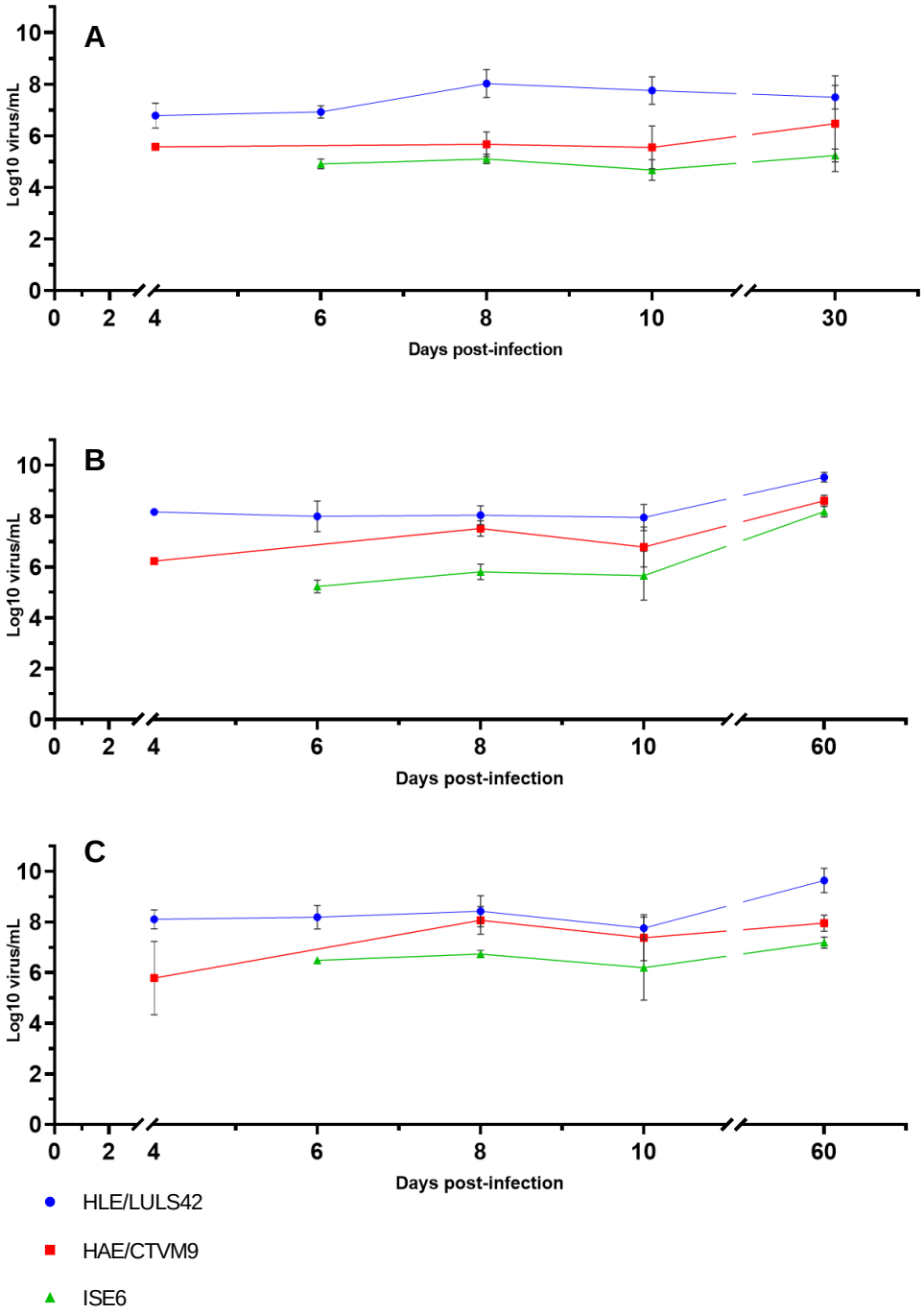

Figure 21. Evolution of HAZV infection in the three tick cell lines used in this study. A- represent the cells infected at MOI 0.1; B – represents cells infected at MOI 1; C cells infected at MOI 5. The different MOIs used are represented by distinct colour. Throughout all time points at MOI 0.1 and 1, HAZV viral titres in HLE/LULS42 cells are significantly higher than those found in the ISE6 cell line. Notably, at 4 dpi, in all three MOIs, the HAZV viral titre in HLE/LULS42 was considerably higher than the viral titre achieved by HAE/CTVM9-HAZV infected cells. (The error bars represent S.D.).

4. Discussion

CCHFV is a major threat responsible for a severe haemorrhagic fever disease and being the most geographically widespread TBV. The recent onset of outbreaks and new detections highlight the need for a better understanding of this Nairovirus circulation and, more importantly, of the tick-CCHFV interactions (Spengler et al., 2018). The (re)emergence of CCHFV increased the interest in studying the impact of the vector in virus maintenance and, also on the role of the tick cellular response to infection and its intrinsic ability to hamper viral replication and control the infection (Belobo et al., 2021; Hart and Thangamani, 2021; Kuehnert et al., 2021).

This work focused mainly in characterizing a viral infection in tick-derived cell lines, comparing the evolution of HAZV infection and establish baseline results for further research. HAZV was chosen was a valid surrogate model for CCHFV, enabling using BSL2 conditions, instead of BSL4 required for CCHFV manipulation. At the time of writing, this is the first study to characterize infection kinetics in a *H. lusitanicum* cell line. Unfortunately, there is no *H. marginatum* derived cell line available for tick research and more time is needed to establish a tick cell line, an effort impossible for this project. As mentioned earlier, *H. lusitanicum* was previously found infected with CCHFV in Spain, pointing out that this tick species may play an important role in CCHFV circulation in the Iberian Peninsula (Moraga-Fernández et al., 2021; Sánchez-Seco et al., 2022). This work has clearly demonstrated that HLE/LULS42 cells produced higher viral titres and showed faster kinetics of replication when comparing with previous results obtained for *H. anatolicum* cells (HAE/CTVM9) infected with HAZV (Salvati et al., 2021). Nonetheless, results revealed a successful infection and establishment of a persistent infection in both cell lines (HLE/LULS42 and HAE/CTVM9).

The first chapter of this thesis is related to HAZV and infection of mammalian cell lines. In the literature, HAZV has been cultured for viral stock production in either SW-13 cells (Hartlaub et al., 2020; Leech, 2015; Matsumoto et al., 2018; Molinas et al., 2016; Salvati et al., 2021; Surtees et al., 2016), or using Baby hamster kidney-21 (BHK-21) cells (Flusin et al., 2011; Foulke et al., 1981; Fuller et al., 2019b; Kalkan-Yazıcı et al., 2021). Nonetheless, no evidence was found of the use of Vero E6 cell for HAZV growth

and propagation. As previously stated, Vero E6 were the only mammalian cell line available for immediate use at IHMT and have been defined as highly permissive to CCHFV infection (Dai et al., 2021). Thus, it was decided to use this mammalian cell line for viral production. Vero E6 were found to be susceptible to HAZV infection and achieved considerable high viral titres (Figure 10), enabling their use for HAZV stock production. Later infections of SW-13 cells with HAZV achieved a higher viral titre comparably with Vero E6, especially on 3 and 4 dpi, where the difference is 2 log higher in SW-13 cells (Figure 12).

Regarding viral infection in mammalian cells, it is important to note that A549 have been widely used in CCHFV studies (Andersson et al., 2008; Garrison et al., 2013; Spengler et al., 2015) and were even used to constitute CCHFV viral stock (Földes et al., 2020a). This cell line displays a permissive behaviour to CCHFV infection. While its use in this thesis comprised only a MOI assay where the objective was to find if this cell line was capable being used for plaque assays, which revealed that, A549 cell do not present any strong visible sign of CPE when infected with HAZV (as described in the studies that used CCHFV), the use of this specific cell line should not be understated. A549 cells have been used as template for study of small interfering RNA (siRNA) targeting CCHFV viral replication (Földes et al., 2020a), highlighting their potential use in subsequent *in vitro* assays with tick-derived cell lines.

The data obtained from the MOI assay with SW-13 cells reveals that after 3 dpi the viral titre stabilizes around 10 logs of virus per mL (Figure 12), suggesting that the peak of viral production is achieved between the second and third dpi. This data is confirmed by assessing that the onset of cellular apoptosis begins 48 hours post infection and is visible by the formation of clear sign of CPE in SW-13 infected cells. These observations are corroborated by previous work in Matsumoto et al., (2019). In this work, it was decided to perform a freeze-thawing step on the adherent SW-13 cells to recover intracellular forms of HAZV. At 4 dpi, the samples with the intracellular forms of the virus had the same viral titre as the supernatant samples. This suggests that the majority of cells had already suffered apoptosis and released HAZV virions in the media at 4 dpi. On the other hand, the intracellular viral forms samples collected at 2 dpi showed a significant ($p < 0.005$) difference between the supernatant collected samples. A higher viral titre (of 2 log difference) was found in the samples that

underwent the freeze-thawing step. This significant increase in the extracellular genome load at 2 dpi, was also found in another studied with CCHFV-infected SW-13 cells (Földes et al., 2020b). Detailed observation of HAZV-infected SW-13 cells (Figure 11) show that, despite visible CPE, the cell monolayer has not suffered apoptosis in its totality, a sign that viral replication as presumably not reached its peak. The results obtained here are in line with previous work describing detection of active apoptosis-inducing caspases abundantly at 48 and 72 hours post infection in HAZV-infected SW-13 cells (Fuller et al., 2019a). Only after 48 hours post infection, SW-13 cells display clear sign of active CPE. As a result, it is expected that by freeze-thawing the cells, and subsequent detachment and destruction of cells integrity, a much higher viral load is detected.

Finally, although A549 and Caco-2 cells were infected with HAZV using the same MOI assay as for Vero E6 and SW-13 cells, unfortunately, due to time and budget restrictions, it was not possible to analyse the samples and determine viral titres. Despite this, both A549 and Caco-2 cells have been used in CCHFV research. As mentioned above A549 cells displayed a valid template for siRNAs viral replication inhibition assays (Földes et al., 2020a). Caco-2 cells have been employed in the study of CCHFV cell tropism and the molecular pathogenesis of CCHFV and HAZV in early stages of infection (Monteil et al., 2020).

The absence of CPE in Vero E6 cells and subsequent absence of viral plaques was a clear obstacle at the beginning of this thesis (Figure 14). Viral titration through plaque assay represents the gold standard to quantify competent viral particles and is still routinely used in virology (Baer and Kehn-Hall, 2014). The virus suppliers assured that HAZV could be cultivated in Vero E6 and that that cell line was could also be used for viral titration. Previous studies showed that Vero E6 cells can be used for viral titration using immunofluorescence assay (Andersson et al., 2004; Salvati et al., 2021; Shepherd et al., 1986) whereas viral plaque assay is only used to quantify HAZV when using SW-13 cell line as template (Fuller et al., 2020; Matsumoto et al., 2018). Besides thorough literature revision, still no clear explanation or direct evidence for this difference between cell lines in HAZV plaque formation was found.

Although Vero E6 cells are described being used as template for standard plaque assay on CCHFV, producing complete CPE (usually in three to four dpi) (Paragas et al., 2004), SW-13 are known to be highly permissible for CCHFV infection and express extensive CPE (Dai et al., 2021) and produce clearly discernible plaques (Bergeron et

al., 2015; Paragas et al., 2004). As discovered in this work the same extrapolation cannot be made for HAZV. The failure of HAZV to induce CPE in Vero E6 could possibly be attributed to different innate immune responses present in that cell strain. As stated, Vero E6 cell are derived from kidney of African green monkey, while SW-13 come from a human adrenal cortex carcinoma line. This difference on the species origin off the cells, may explain this result. A previous study conducted with human and bovine cells infected with CCHFV, suggested that cellular tropism variation on the virus are related to the different host factors and innate cellular mechanisms (Földes et al., 2020b). Recent work with HAZV found that the N protein of the virus plays a role in viral propagation in mammalian cells by inhibit apoptosis (Matsumoto et al., 2019). Strangely, CCHFV has showed to induce apoptosis in mammalian cell lines via expression of the non-structural accessory protein NSs (expressed via ambisense transcription within the S segment) (Barnwal et al., 2016). Recently, the same mechanism of apoptosis inducer via N-protein was found in HAZV (Fuller et al., 2019a). The possibility is open that, non-structural elements of the S segment of Nairoviruses, such as the accessory NSs protein from CCHFV, may play a regulation function on the innate immune systems. It is also feasible that, these accessory proteins could only interact with specific component of a host that may not be present in other cells. One such hypothesis could explain the distinct pathological effect displayed by HAZV in Vero E6 cells and in SW-13 cells.

The optimization of the protocol for plaque assay for HAZV quantification led to the use of two distinct overlay media: agarose and CMC. The main difference relied on plaque morphology. The CMC overlay presented small plaques, while the use of agarose led to the formation of larger plaques (Figure 15), possibly hinting at lower viral inhibition. Agarose plates had to be performed in 6-well plates since the large size of the viral plates created border diffusion and were difficult to count. In this work, the use of agarose as overlay resulted in clearer plaques and achieved a higher particle count, only 1 order of magnitude lower (log10) than the viral quantification rendered by RT-qPCR. While the use of CMC as overlay provided an easier approach, it also displayed 1,5 and 2 orders of magnitude lower (log10), for CMC 2% and CMC 3% respectively, than viral genome counts obtained by RT-qPCR. Other studies, conducted with other viruses, also reported lower viral titres when using CMC as overlay medium (Baer and

Kehn-Hall, 2014; Juarez et al., 2013). Even tough sensitivity of the assay slightly decreases when using CMC as overlay, the formation of reduced plaque sizes can be beneficial when working with faster replication viruses. Furthermore, decreasing the concentration of the overlay medium to 1 % (or even lower) or extending the duration of the incubation period to ensure propagation of infection, enabling bigger and distinct viral plaques, may be suggested.

The new TaqMan® based RT-qPCR assay design for this thesis enabled a fast method for HAZV detection and proved to be a reliable option to determine the viral genome equivalents in each sample. The use of gBlocks® as template for standard curves proved to be a very versatile solution as it was simple to prepare and enable a reduction of costs and time by not having to develop an internal control for assay calibration.

With the main goal of describing the evolution of HAZV infection, three distinct tick cell lines were chosen to be tested and compared. The ISE6 cell line was the first used in HAZV studies and demonstrated capacity to support the viral replication. The study also revealed a slower rate of viral growth in ISE6 cells compared to mammalian cells (BHK-21 cells) (Garcia et al., 2005). Currently, cell lines derived from *H. anatolicum* have become increasingly used since they belong to the genus *Hyalomma* which is regarded as the main vector for CCHFV. The tick cell lines HAE/CTVM8 and HAE/CTVM9, both originated from embryonic tissues of *H. anatolicum* (Bell-Sakyi, 1991), have been used in CCHFV research (Salata et al., 2018) being both cell lines permissive to infection. Later, HAE/CTVM9 cells were reported to enable replication of HAZV (Fuller et al., 2019a). Therefore, an *in vitro* infection model based on both HAE/CTVM9 and ISE6 cells was already described and used for tick research. Recently, a new tick cell line originated from *H. lusitanicum* egg batches - HLE/LULS42 – was described (Bell-Sakyi et al., 2022). Since CCHFV was found in *H. lusitanicum* ticks and the vector itself is widely distributed in the Iberian Peninsula and other southern European regions (Estrada-Peña et al., 2012; Portillo et al., 2021; Sánchez-Seco et al., 2022), this tick cell line became of great interest to be used in this thesis work.

This thesis is the first work to find that HAZV is able to replicate in HLE/LULS42 cell line without displaying any visible sign of CPE. Consistent detection of HAZV up to two months after infection in all three tick cell lines revels that HAZV persistently infects tick

cell lines (Figures 18, 19 and 20). This persistent infection had already been reported in ISE6 cells using other TBV (Rückert, 2014; Weisheit, 2014) and in HAE/CTVM9 with HAZV (Salvati et al., 2021).Nonetheless, this is the first description of a HAZV persistent infection in a *H. lusitanicum* derived cell line, without apparent fitness cost for this tick cell line.

Previous work conducted by Bell-Sakyi et al.(2012), analysed different tick cell lines from five distinct genus (*Hyalomma, Ixodes, Amblyomma, Rhipicephalus* and *Ornithodoros*) concluded that the two cell lines derived from *H. anatolicum* revealed the higher susceptibility. In this work, both HAE/CTVM9 and HLE/LULS42 cell lines showed higher viral titres in each of the three MOIs used compared to ISE6 cell line. Remarkably, the HLE/LULS42 cell line also produced higher viral titres than HAE/CTVM9, despite both being derived from ticks of the same genus. This difference was present in all the three MOIs at 4 dpi suggesting that viral replication takes place at a higher rate in HLE/LULS42 cells, hence rendering higher viral titres. Secondly, this difference is also present at 8 dpi, where all three cell lines achieved their peak viral concentration. The viral titres detected at HLE/LULS42 cells were significantly higher than the other two cell lines, further corroborating that the kinetics of viral progeny release are different (Figure 21). In conclusion, the production of detectable HAZV particles happens faster and in bigger quantity in *H. lusitanicum* derived cell lines. These results illustrate the complexity of tick-virus interactions and the importance of vector competence for each virus replication.

Recent work described the detection of viral-derived DNA forms (vDNA) from HAZV in HAE/CTVM9 cells infected with HAZV. The authors suggested that vDNA has an impact on virus replication by means of downregulation, playing a key role in the equilibrium of the mechanisms controlling infection (Salvati et al., 2021). Considering that the intrinsic tick mechanisms allowing the establishment of a persistent viral infection are still unexplained, this vDNA continuous production may represent a possible new tool for vector control, enabling further research on the strategies displayed by vectors on controlling replication of RNA viruses such as HAZV and CCHFV. Although the work developed in this thesis did not incorporate the study of vDNAs, it is clear that should be taken into account in future studies. Furthermore, it is highly plausible that vDNAs are also present in HLE/LULS42 cells and may play a role

in controlling infection. While the formation of a persistent infection in ticks results in their ability to control the dynamics of infection, further studies are needed to understand the impact of the host immunity in the maintenance of the infection. Moreover, the role of RNA interference (RNAi) in the modulation the immune response of viral infections may play a role in the tick antiviral response (Hart and Thangamani, 2021; Talactac et al., 2021). Another factor to consider regarding the persistence infection in tick cell lines is the selective pressure on viral populations and how the tick-virus interactions modulate the selection of viral variants less likely to hamper tick growth. There is a lack of experimental studies to elucidate the role of not only vDNAs but also the tick innate immune system in the virus-vector interactions. As aforementioned, the innate cellular response of inducing apoptosis, in both CCHFV and HAZV infected mammalian cells, points to a Nairovirus viral multiplication feature present in mammalian cells but not tick cell lines. Encompassing the study of vDNAs and the role of non-structural proteins from the S segment of CCHFV should be investigated in the future. Therefore, there is a need for more data to enlighten these elusive antiviral responses that are critical for understanding the maintenance and transmission of TBV.

The detection of vDNAs and further analysis, should be carried out in future work conducted with HLE/LULS42 cells. Additionally, as vDNAs enable the survival of infected ticks by suppression of viral replication using a modulation tactic, RNAi future studies should be conducted. As such, analysis of expression of micro-RNAs (miRNAs) targeting viral RNA sequences should be carried out in the future, using gene silencing with RNAi techniques. Firstly, an *in silico* approach to assess miRNAs targets on the tick genome and also on HAZV should be performed. An ongoing project being conducted at IHMT aims to sequence the full genome of *H. marginatum* which would be a great asset in identifying possible relevant genes for controlling viral infection. Using *H. lusitanicum* derived cell lines will enable to extrapolate the data obtained from the genome analysis of *H. marginatum,* as this two tick species are closely related, and both are vector for CCHFV. Furthermore, it is of major interest to progress from an *in vitro* system and develop an *in vivo* infection study system using *H. lusitanicum* ticks.

While some advances have been made, namely the vector competence of *Ixodes ricinus* ticks for both HAZV and CCHFV transmission (Leech, 2015), there is still a scarcity of fully tested and proven *in vivo* models and experimental protocols for infection monitoring and analysis. With that in mind, this thesis results attest the use of

H. lusitanicum derived cell lines for *in vitro* assays and open the possibility of using the same tick species as template for an *in vivo* system where the application of RNAi genomic tools should be considered as the next step for CCHFV-tick interactions studies.

5. Concluding remarks and final perspectives

HAZV was able to infect all the three tick cell lines used, producing higher viral titres in HLE/LULS42 cells. Moreover, the virus did not induce any cytopathic effect in the tick cell lines and the infection persisted throughout the duration of the experiment.

This novel *H. lusitanicum* derived cell line shows a tremendous potential to become a standard tick cell line to study tick-HAZV interactions to extrapolate results to CCHFV and, subsequently, to hamper CCHFV transmission and improving TBV control.

RNAi techniques should be carried out in an *in vitro* system, using HLE/LULS42 cells, before extrapolating to an in vivo model. In addition, development of targeted gene silencing assays against tick genes with a possible effect on viral replication should be carried out. This will enable to provide a guide for future studies on vector-pathogen interaction and enlighten our knowledge on CCHFV.

6. Bibliography

Adams, G., 2020. A beginner's guide to RT-PCR, qPCR and RT-qPCR. The Biochemist 42, 48–53. https://doi.org/10.1042/BIO20200034

Al-Rofaai, A., Bell-Sakyi, L., 2020. Tick Cell Lines in Research on Tick Control. Front. Physiol. 11.

Andersson, I., Bladh, L., Mousavi-Jazi, M., Magnusson, K.-E., Lundkvist, Å., Haller, O., Mirazimi, A., 2004. Human MxA Protein Inhibits the Replication of Crimean-Congo Hemorrhagic Fever Virus. J. Virol. 78, 4323–4329. https://doi.org/10.1128/JVI.78.8.4323-4329.2004

Andersson, I., Karlberg, H., Mousavi-Jazi, M., Martínez-Sobrido, L., Weber, F., Mirazimi, A., 2008. Crimean-Congo hemorrhagic fever virus delays activation of the innate immune response. J. Med. Virol. 80, 1397–1404. https://doi.org/10.1002/jmv.21222

Andersson, I., Lundkvist, Å., Haller, O., Mirazimi, A., 2006. Type I interferon inhibits Crimean-Congo hemorrhagic fever virus in human target cells. J. Med. Virol. 78, 216–222. https://doi.org/10.1002/jmv.20530

Arteaga, L.M., Bellido, J.L.M., Lista, M.C.V., Santiago, M.B.V., Soto, P.F., Bas, I., Leralta, N., Manchón, F. de O., Negredo, A.I., Seco, M.P.S., Sardón, M.A., González, S.P., Bianco, A.J. del, Peris, L.B., Alamo-Sanz, R., Hewson, R., Belhassen-García, M., Muro, A., 2020. Crimean-Congo haemorrhagic fever (CCHF) virus-specific antibody detection in blood donors, Castile-León, Spain, summer 2017 and 2018. Eurosurveillance 25, 1900507. https://doi.org/10.2807/1560-7917.ES.2020.25.10.1900507

Arteaga, L.M., Bellido, J.L.M., Negredo, A.I., Criado, J.G., Lista, M.C.V., Serrano, J.Á.S., Santiago, M.B.V., Bernús, A.L., Manchón, F. de O., Seco, M.P.S., Leralta, N., Sardón, M.A., Muro, A., Belhassen-García, M., 2021. New circulation of genotype V of Crimean-Congo haemorrhagic fever virus in humans from Spain. PLoS Negl. Trop. Dis. 15, e0009197. https://doi.org/10.1371/journal.pntd.0009197

Atkinson, B., Chamberlain, J., Logue, C.H., Cook, N., Bruce, C., Dowall, S.D., Hewson, R., 2012. Development of a real-time RT-PCR assay for the detection of Crimean-Congo hemorrhagic fever virus. Vector Borne Zoonotic Dis. Larchmt. N 12, 786–793. https://doi.org/10.1089/vbz.2011.0770

Baer, A., Kehn-Hall, K., 2014. Viral Concentration Determination Through Plaque Assays: Using Traditional and Novel Overlay Systems. JoVE J. Vis. Exp. e52065. https://doi.org/10.3791/52065

Bandeira, L. m., Puga, M. a. m., de Paula, V. s., Demarchi, L. h. f., Lichs, G. g. c., Domingos, J. a., da Cunha, R. v., Uehara, S. n. o., Motta-Castro, A. r. c., 2020. Use of synthetic oligonucleotides for determination of HTLV-1 proviral load by real-time PCR: a helpful alternative approach in the clinical management. J. Appl. Microbiol. 129, 768–774. https://doi.org/10.1111/jam.14646

Barandika, J.F., Olmeda, S.A., Casado-Nistal, M.A., Hurtado, A., Juste, R.A., Valcárcel, F., Anda, P., García-Pérez, A.L., 2011. Differences in Questing Tick Species Distribution Between Atlantic and Continental Climate Regions in Spain. J. Med. Entomol. 48, 13–19. https://doi.org/10.1603/ME10079

Barnwal, B., Karlberg, H., Mirazimi, A., Tan, Y.-J., 2016. The Non-structural Protein of Crimean-Congo Hemorrhagic Fever Virus Disrupts the Mitochondrial Membrane

Potential and Induces Apoptosis *. J. Biol. Chem. 291, 582–592. https://doi.org/10.1074/jbc.M115.667436
Begum, F., Wisseman, C.L., Jr., Casals, J., 1970. Tick-Borne Viruses of West Pakistan: Ii. Hazara Virus, A New Agent Isolated from Ixodes Redikorzeviticks from The Kaghan Valley, W. Pakistan12. Am. J. Epidemiol. 92, 192–194. https://doi.org/10.1093/oxfordjournals.aje.a121197
Bell-Sakyi, L., 1991. Continuous cell lines from the tick Hyalomma anatolicum anatolicum. J. Parasitol. 77, 1006–1008.
Bell-Sakyi, L., Hartley, C.S., Khoo, J.J., Forth, J.H., Palomar, A.M., Makepeace, B.L., 2022. New Cell Lines Derived from European Tick Species. Microorganisms 10, 1086. https://doi.org/10.3390/microorganisms10061086
Bell-Sakyi, L., Kohl, A., Bente, D.A., Fazakerley, J.K., 2012. Tick Cell Lines for Study of Crimean-Congo Hemorrhagic Fever Virus and Other Arboviruses. Vector Borne Zoonotic Dis. 12, 769–781. https://doi.org/10.1089/vbz.2011.0766
Bell-Sakyi, L., Zweygarth, E., Blouin, E.F., Gould, E.A., Jongejan, F., 2007. Tick cell lines: tools for tick and tick-borne disease research. Trends Parasitol., Tick-host-pathogen interactions in the post-genomic era 23, 450–457. https://doi.org/10.1016/j.pt.2007.07.009
Belobo, J.T.E., Kenmoe, S., Kengne-Nde, C., Emoh, C.P.D., Bowo-Ngandji, A., Tchatchouang, S., Wobessi, J.N.S., Mikangue, C.A.M., Tazokong, H.R., Bebey, S.R.K., Noura, E.A., Ka'e, A.C., Simo, R.E.G., Modiyinji, A.F., Ngongang, D.T., Che, E., Kenfack, S., Nzukui, N.D., Adjia, N.A., Babassagana, I.T., Mahamat, G., Mbaga, D.S., Mbacham, W.F., Sadeuh-Mbah, S.A., Njouom, R., 2021. Worldwide epidemiology of Crimean-Congo Hemorrhagic Fever Virus in humans, ticks and other animal species, a systematic review and meta-analysis. PLoS Negl. Trop. Dis. 15, e0009299. https://doi.org/10.1371/journal.pntd.0009299
Bente, D.A., Alimonti, J.B., Shieh, W.-J., Camus, G., Ströher, U., Zaki, S., Jones, S.M., 2010. Pathogenesis and immune response of Crimean-Congo hemorrhagic fever virus in a STAT-1 knockout mouse model. J. Virol. 84, 11089–11100. https://doi.org/10.1128/JVI.01383-10
Bente, D.A., Forrester, N.L., Watts, D.M., McAuley, A.J., Whitehouse, C.A., Bray, M., 2013. Crimean-Congo hemorrhagic fever: History, epidemiology, pathogenesis, clinical syndrome and genetic diversity. Antiviral Res. 100, 159–189. https://doi.org/10.1016/j.antiviral.2013.07.006
Bereczky, S., Lindegren, G., Karlberg, H., Akerstrom, S., Klingstrom, J., Mirazimi, A., 2010. Crimean-Congo hemorrhagic fever virus infection is lethal for adult type I interferon receptor-knockout mice. J. Gen. Virol. 91, 1473–1477. https://doi.org/10.1099/vir.0.019034-0
Bergeron, É., Zivcec, M., Chakrabarti, A.K., Nichol, S.T., Albariño, C.G., Spiropoulou, C.F., 2015. Recovery of Recombinant Crimean Congo Hemorrhagic Fever Virus Reveals a Function for Non-structural Glycoproteins Cleavage by Furin. PLOS Pathog. 11, e1004879. https://doi.org/10.1371/journal.ppat.1004879
Blumberg, L., Enria, D., Bausch, D.G., 2014. 16 - Viral Haemorrhagic Fevers, in: Farrar, J., Hotez, P.J., Junghanss, T., Kang, G., Lalloo, D., White, N.J. (Eds.), Manson's Tropical Infectious Diseases (Twenty-Third Edition). W.B. Saunders, London, pp. 171-194.e2. https://doi.org/10.1016/B978-0-7020-5101-2.00017-0

Bustin, S., 2000. Absolute quantification of mRNA using real-time reverse transcription polymerase chain reaction assays. J. Mol. Endocrinol. 25, 169–193. https://doi.org/10.1677/jme.0.0250169

Cajimat, M.N.B., Rodriguez, S.E., Schuster, I.U.E., Swetnam, D.M., Ksiazek, T.G., Habela, M.A., Negredo, A.I., Estrada-Peña, A., Barrett, A.D.T., Bente, D.A., 2017. Genomic Characterization of Crimean–Congo Hemorrhagic Fever Virus in Hyalomma Tick from Spain, 2014. Vector-Borne Zoonotic Dis. 17, 714–719. https://doi.org/10.1089/vbz.2017.2190

Casals, J., 1969. Antigenic Similarity between the Virus Causing Crimean Hemorrhagic Fever and Congo Virus. Proc. Soc. Exp. Biol. Med. 131, 233–236. https://doi.org/10.3181/00379727-131-33847

Casals, J., Tignor, G.H., 1980. The Nairovirus Genus: Serological Relationships. Intervirology 14, 144–147. https://doi.org/10.1159/000149175

Casals, J., Tignor, G.H., 1974. Neutralization and Hemagglutination-Inhibition Tests with Crimean Hemorrhagic Fever-Congo Virus. Proc. Soc. Exp. Biol. Med. 145, 960–966. https://doi.org/10.3181/00379727-145-37933

Centro de Estudos de Vetores e Doenças Infeciosas Doutor Francisco Cambournac, 2022. Relatório REVIVE 2021 - Culicídeos e Ixodídeos: Rede de Vigilância de Vetores (report). Instituto Nacional de Saúde Doutor Ricardo Jorge, IP.

Clementi, M., Menzo, S., Bagnarelli, P., Manzin, A., Valenza, A., Varaldo, P.E., 1993. Quantitative PCR and RT-PCR in virology. Genome Res. 2, 191–196. https://doi.org/10.1101/gr.2.3.191

Conte, J., Potoczniak, M.J., Tobe, S.S., 2018. Using synthetic oligonucleotides as standards in probe-based qPCR. BioTechniques 64, 177–179. https://doi.org/10.2144/btn-2018-2000

Cui, M., Zhou, H., Zhang, B., Carr, M.J., Guo, M., Shi, W., 2022. Rapid detection of the emerging tick-borne Tamdy virus by TaqMan-based real-time reverse transcription PCR. J. Virol. Methods 305, 114538. https://doi.org/10.1016/j.jviromet.2022.114538

Dai, S., Wu, Q., Wu, X., Peng, C., Liu, J., Tang, S., Zhang, T., Deng, F., Shen, S., 2021. Differential Cell Line Susceptibility to Crimean-Congo Hemorrhagic Fever Virus. Front. Cell. Infect. Microbiol. 11. https://doi.org/10.3389/fcimb.2021.648077

De Paula, S.O., de Melo Lima, C., Torres, M.P., Pereira, M.R.G., Lopes da Fonseca, B.A., 2004. One-Step RT-PCR protocols improve the rate of dengue diagnosis compared to Two-Step RT-PCR approaches. J. Clin. Virol. 30, 297–301. https://doi.org/10.1016/j.jcv.2003.11.004

Dickson, D.L., Turell, M.J., 1992. Replication and tissue tropisms of Crimean-Congo hemorrhagic fever virus in experimentally infected adult Hyalomma truncatum (Acari: Ixodidae). J. Med. Entomol. 29, 767–773. https://doi.org/10.1093/jmedent/29.5.767

Dowall, S.D., Carroll, M.W., Hewson, R., 2017. Development of vaccines against Crimean-Congo haemorrhagic fever virus. Vaccine, Biosecurity 35, 6015–6023. https://doi.org/10.1016/j.vaccine.2017.05.031

Drosten, C., Göttig, S., Schilling, S., Asper, M., Panning, M., Schmitz, H., Günther, S., 2002. Rapid Detection and Quantification of RNA of Ebola and Marburg Viruses, Lassa Virus, Crimean-Congo Hemorrhagic Fever Virus, Rift Valley Fever Virus, Dengue Virus, and Yellow Fever Virus by Real-Time Reverse Transcription-PCR. J. Clin. Microbiol. 40, 2323–2330. https://doi.org/10.1128/JCM.40.7.2323-2330.2002

Durden, L.A., Logan, T.M., Wilson, M.L., Linthicum, K.J., 1993. Experimental Vector Incompetence of a Soft Tick, Ornithodoros sonrai (Acari: Argasidae), for

Crimean-Congo Hemorrhagic Fever Virus. J. Med. Entomol. 30, 493–496. https://doi.org/10.1093/jmedent/30.2.493

Ergonul, O., 2012. Crimean–Congo hemorrhagic fever virus: new outbreaks, new discoveries. Curr. Opin. Virol., Virus structure and function / Emerging viruses 2, 215–220. https://doi.org/10.1016/j.coviro.2012.03.001

Estrada-Peña, A., Palomar, A.M., Santibáñez, P., Sánchez, N., Habela, M.A., Portillo, A., Romero, L., Oteo, J.A., 2012. Crimean-Congo Hemorrhagic Fever Virus in Ticks, Southwestern Europe, 2010. Emerg. Infect. Dis. 18, 179–180. https://doi.org/10.3201/eid1801.111040

Filipe, A.R., Calisher, C.H., Lazuick, J., 1985. Antibodies to Congo-Crimean haemorrhagic fever, Dhori, Thogoto and Bhanja viruses in southern Portugal. Acta Virol. 29, 324–328.

Flusin, O., Vigne, S., Peyrefitte, C.N., Bouloy, M., Crance, J.-M., Iseni, F., 2011. Inhibition of Hazara nairovirus replication by small interfering RNAs and their combination with ribavirin. Virol. J. 8, 249. https://doi.org/10.1186/1743-422X-8-249

Földes, F., Madai, M., Papp, H., Kemenesi, G., Zana, B., Geiger, L., Gombos, K., Somogyi, B., Bock-Marquette, I., Jakab, F., 2020a. Small Interfering RNAs Are Highly Effective Inhibitors of Crimean-Congo Hemorrhagic Fever Virus Replication In Vitro. Molecules 25, 5771. https://doi.org/10.3390/molecules25235771

Földes, K., Aligholipour Farzani, T., Ergünay, K., Ozkul, A., 2020b. Differential Growth Characteristics of Crimean-Congo Hemorrhagic Fever Virus in Kidney Cells of Human and Bovine Origin. Viruses 12, 685. https://doi.org/10.3390/v12060685

Foulke, R.S., Rosato, R.R., French, G.R., 1981. Structural polypeptides of Hazara virus. J. Gen. Virol. 53, 169–172. https://doi.org/10.1099/0022-1317-53-1-169

Fuller, J., Álvarez-Rodríguez, B., Todd, E.J.A.A., Mankouri, J., Hewson, R., Barr, J.N., 2020. Hazara Nairovirus Requires COPI Components in both Arf1-Dependent and Arf1-Independent Stages of Its Replication Cycle. J. Virol. 94, e00766-20. https://doi.org/10.1128/JVI.00766-20

Fuller, J., Surtees, R.A., Shaw, A.B., Álvarez-Rodríguez, B., Slack, G.S., Bell-Sakyi, L., Mankouri, J., Edwards, T.A., Hewson, R., Barr, J.N., 2019a. Hazara nairovirus elicits differential induction of apoptosis and nucleocapsid protein cleavage in mammalian and tick cells. J. Gen. Virol. 100, 392–402.

Fuller, J., Surtees, R.A., Slack, G.S., Mankouri, J., Hewson, R., Barr, J.N., 2019b. Rescue of Infectious Recombinant Hazara Nairovirus from cDNA Reveals the Nucleocapsid Protein DQVD Caspase Cleavage Motif Performs an Essential Role other than Cleavage. J. Virol. 93, e00616-19. https://doi.org/10.1128/JVI.00616-19

Garcia, S., Billecocq, A., Crance, J.-M., Munderloh, U., Garin, D., Bouloy, M., 2005. Nairovirus RNA Sequences Expressed by a Semliki Forest Virus Replicon Induce RNA Interference in Tick Cells. J. Virol. 79, 8942–8947. https://doi.org/10.1128/JVI.79.14.8942-8947.2005

Gargili, A., Estrada-Peña, A., Spengler, J.R., Lukashev, A., Nuttall, P.A., Bente, D.A., 2017. The role of ticks in the maintenance and transmission of Crimean-Congo hemorrhagic fever virus: A review of published field and laboratory studies. Antiviral Res. 144, 93–119. https://doi.org/10.1016/j.antiviral.2017.05.010

Garrison, A.R., Alakbarova, S., Kulesh, D.A., Shezmukhamedova, D., Khodjaev, S., Endy, T.P., Paragas, J., 2007. Development of a TaqMan®–Minor Groove

Binding Protein Assay for the Detection and Quantification of Crimean-Congo Hemorrhagic Fever Virus. Am. J. Trop. Med. Hyg. 77, 514–520. https://doi.org/10.4269/ajtmh.2007.77.514

Garrison, A.R., Alkhovsky [Альховский Сергей Владимирович], S.V., Avšič-Županc, T., Bente, D.A., Bergeron, É., Burt, F., Di Paola, N., Ergünay, K., Hewson, R., Kuhn, J.H., Mirazimi, A., Papa [Άννα Παπά], A., Sall, A.A., Spengler, J.R., Palacios, G., Consortium, I.R., 2020. ICTV Virus Taxonomy Profile: Nairoviridae. J. Gen. Virol. 101, 798–799. https://doi.org/10.1099/jgv.0.001485

Garrison, A.R., Radoshitzky, S.R., Kota, K.P., Pegoraro, G., Ruthel, G., Kuhn, J.H., Altamura, L.A., Kwilas, S.A., Bavari, S., Haucke, V., Schmaljohn, C.S., 2013. Crimean–Congo hemorrhagic fever virus utilizes a clathrin- and early endosome-dependent entry pathway. Virology 444, 45–54. https://doi.org/10.1016/j.virol.2013.05.030

Garrison, A.R., Smith, D.R., Golden, J.W., 2019. Animal Models for Crimean-Congo Hemorrhagic Fever Human Disease. Viruses 11, 590. https://doi.org/10.3390/v11070590

Haddock, E., Feldmann, F., Hawman, D.W., Zivcec, M., Hanley, P.W., Saturday, G., Scott, D.P., Thomas, T., Korva, M., Avšič -Županc, T., Safronetz, D., Feldmann, H., 2018. A cynomolgus macaque model for Crimean–Congo haemorrhagic fever. Nat. Microbiol. 3, 556–562. https://doi.org/10.1038/s41564-018-0141-7

Hart, C.E., Thangamani, S., 2021. Tick-virus interactions: Current understanding and future perspectives. Parasite Immunol. 43, e12815. https://doi.org/10.1111/pim.12815

Hartlaub, J., von Arnim, F., Fast, C., Somova, M., Mirazimi, A., Groschup, M.H., Keller, M., 2020. Sheep and Cattle Are Not Susceptible to Experimental Inoculation with Hazara Orthonairovirus, a Tick-Borne Arbovirus Closely Related to CCHFV. Microorganisms 8, 1927. https://doi.org/10.3390/microorganisms8121927

Hawman, David W., Ahlén, G., Appelberg, K.S., Meade-White, K., Hanley, P.W., Scott, D., Monteil, V., Devignot, S., Okumura, A., Weber, F., Feldmann, H., Sällberg, M., Mirazimi, A., 2021. A DNA-based vaccine protects against Crimean-Congo haemorrhagic fever virus disease in a Cynomolgus macaque model. Nat. Microbiol. 6, 187–195. https://doi.org/10.1038/s41564-020-00815-6

Hawman, D.W., Feldmann, H., 2018. Recent advances in understanding Crimean–Congo hemorrhagic fever virus. https://doi.org/10.12688/f1000research.16189.1

Hawman, David W, Meade-White, K., Leventhal, S., Feldmann, F., Okumura, A., Smith, B., Scott, D., Feldmann, H., 2021. Immunocompetent mouse model for Crimean-Congo hemorrhagic fever virus. eLife 10, e63906. https://doi.org/10.7554/eLife.63906

Holland, P.M., Abramson, R.D., Watson, R., Gelfand, D.H., 1991. Detection of specific polymerase chain reaction product by utilizing the 5'----3' exonuclease activity of Thermus aquaticus DNA polymerase. Proc. Natl. Acad. Sci. 88, 7276–7280. https://doi.org/10.1073/pnas.88.16.7276

Hoogstraal, H., 1979. The epidemiology of tick-borne Crimean-Congo hemorrhagic fever in Asia, Europe, and Africa. J. Med. Entomol. 15, 307–417. https://doi.org/10.1093/jmedent/15.4.307

Hubálek, Z., Rudolf, I., 2012. Tick-borne viruses in Europe. Parasitol. Res. 111, 9–36. https://doi.org/10.1007/s00436-012-2910-1

Jalali, Mehdi, Zaborowska, J., Jalali, Morteza, 2017. Chapter 1 - The Polymerase Chain Reaction: PCR, qPCR, and RT-PCR, in: Jalali, Morteza, Saldanha, F.Y.L., Jalali, Mehdi (Eds.), Basic Science Methods for Clinical Researchers.

Academic Press, Boston, pp. 1–18. https://doi.org/10.1016/B978-0-12-803077-6.00001-1
Juarez, D., Long, K.C., Aguilar, P., Kochel, T.J., Halsey, E.S., 2013. Assessment of plaque assay methods for alphaviruses. J. Virol. Methods 187, 185–189. https://doi.org/10.1016/j.jviromet.2012.09.026
Kalkan-Yazıcı, M., Karaaslan, E., Çetin, N.S., Hasanoğlu, S., Güney, F., Zeybek, Ü., Doymaz, M.Z., 2021. Cross-Reactive Anti-Nucleocapsid Protein Immunity against Crimean-Congo Hemorrhagic Fever Virus and Hazara Virus in Multiple Species. J. Virol. 95, e02156-20. https://doi.org/10.1128/JVI.02156-20
Kazimírová, M., Thangamani, S., Bartíková, P., Hermance, M., Holíková, V., Štibrániová, I., Nuttall, P.A., 2017. Tick-Borne Viruses and Biological Processes at the Tick-Host-Virus Interface. Front. Cell. Infect. Microbiol. 7.
Koehler, J.W., Delp, K.L., Hall, A.T., Olschner, S.P., Kearney, B.J., Garrison, A.R., Altamura, L.A., Rossi, C.A., Minogue, T.D., 2018. Sequence Optimized Real-Time Reverse Transcription Polymerase Chain Reaction Assay for Detection of Crimean-Congo Hemorrhagic Fever Virus. Am. J. Trop. Med. Hyg. 98, 211–215. https://doi.org/10.4269/ajtmh.17-0165
Kralik, P., Ricchi, M., 2017. A Basic Guide to Real Time PCR in Microbial Diagnostics: Definitions, Parameters, and Everything. Front. Microbiol. 8.
Kuehnert, P.A., Stefan, C.P., Badger, C.V., Ricks, K.M., 2021. Crimean-Congo Hemorrhagic Fever Virus (CCHFV): A Silent but Widespread Threat. Curr. Trop. Med. Rep. 8, 141–147. https://doi.org/10.1007/s40475-021-00235-4
Kuhn, J.H., Wiley, M.R., Rodriguez, S.E., Bào, Y., Prieto, K., Travassos da Rosa, A.P.A., Guzman, H., Savji, N., Ladner, J.T., Tesh, R.B., Wada, J., Jahrling, P.B., Bente, D.A., Palacios, G., 2016. Genomic Characterization of the Genus Nairovirus (Family Bunyaviridae). Viruses 8, 164. https://doi.org/10.3390/v8060164
Kutyavin, I.V., Afonina, I.A., Mills, A., Gorn, V.V., Lukhtanov, E.A., Belousov, E.S., Singer, M.J., Walburger, D.K., Lokhov, S.G., Gall, A.A., Dempcy, R., Reed, M.W., Meyer, R.B., Hedgpeth, J., 2000. 3′-Minor groove binder-DNA probes increase sequence specificity at PCR extension temperatures. Nucleic Acids Res. 28, 655. https://doi.org/10.1093/nar/28.2.655
Labuda, M., Nuttall, P.A., 2004. Tick-borne viruses. Parasitology 129, S221–S245. https://doi.org/10.1017/S0031182004005220
Lasecka, L., Baron, M.D., 2014. The molecular biology of nairoviruses, an emerging group of tick-borne arboviruses. Arch. Virol. 159, 1249–1265. https://doi.org/10.1007/s00705-013-1940-z
Leech, S.L., 2015. Investigation into the vector competence of Ixodes ricinus ticks to Hazara virus and Crimean-Congo Haemorrhagic Fever virus (doctoral). London School of Hygiene & Tropical Medicine. https://doi.org/10.17037/PUBS.02212902
Lewandowski, K., Bell, A., Miles, R., Carne, S., Wooldridge, D., Manso, C., Hennessy, N., Bailey, D., Pullan, S.T., Gharbia, S., Vipond, R., 2017. The Effect of Nucleic Acid Extraction Platforms and Sample Storage on the Integrity of Viral RNA for Use in Whole Genome Sequencing. J. Mol. Diagn. 19, 303–312. https://doi.org/10.1016/j.jmoldx.2016.10.005
Mackay, I.M., Arden, K.E., Nitsche, A., 2002. Real-time PCR in virology. Nucleic Acids Res. 30, 1292–1305. https://doi.org/10.1093/nar/30.6.1292

Mansfield, K.L., Jizhou, L., Phipps, L.P., Johnson, N., 2017. Emerging Tick-Borne Viruses in the Twenty-First Century. Front. Cell. Infect. Microbiol. 7.

Marthaler, D., Homwong, N., Rossow, K., Culhane, M., Goyal, S., Collins, J., Matthijnssens, J., Ciarlet, M., 2014. Rapid detection and high occurrence of porcine rotavirus A, B, and C by RT-qPCR in diagnostic samples. J. Virol. Methods 209, 30–34. https://doi.org/10.1016/j.jviromet.2014.08.018

Matsumoto, Y., Nouchi, T., Ohta, K., Nishio, M., 2019. Regulation of Hazara virus growth through apoptosis inhibition by viral nucleoprotein. Arch. Virol. 164, 1597–1607. https://doi.org/10.1007/s00705-019-04236-7

Matsumoto, Y., Ohta, K., Nishio, M., 2018. Lethal infection of embryonated chicken eggs by Hazara virus, a model for Crimean-Congo hemorrhagic fever virus. Arch. Virol. 163, 219–222. https://doi.org/10.1007/s00705-017-3580-1

Mehand, M.S., Al-Shorbaji, F., Millett, P., Murgue, B., 2018. The WHO R&D Blueprint: 2018 review of emerging infectious diseases requiring urgent research and development efforts. Antiviral Res. 159, 63–67. https://doi.org/10.1016/j.antiviral.2018.09.009

Mendoza, E.J., Warner, B., Safronetz, D., Ranadheera, C., 2018. Crimean–Congo haemorrhagic fever virus: Past, present and future insights for animal modelling and medical countermeasures. Zoonoses Public Health 65, 465–480. https://doi.org/10.1111/zph.12469

Mertens, M., Schmidt, K., Ozkul, A., Groschup, M.H., 2013. The impact of Crimean-Congo hemorrhagic fever virus on public health. Antiviral Res. 98, 248–260. https://doi.org/10.1016/j.antiviral.2013.02.007

Molinas, A., Mirazimi, A., Holm, A., Loitto, V.M., Magnusson, K.-E., Vikström, E., 2016. Protective role of host aquaporin 6 against Hazara virus, a model for Crimean–Congo hemorrhagic fever virus infection. FEMS Microbiol. Lett. 363, fnw058. https://doi.org/10.1093/femsle/fnw058

Monteil, V., Salata, C., Appelberg, S., Mirazimi, A., 2020. Hazara virus and Crimean-Congo Hemorrhagic Fever Virus show a different pattern of entry in fully-polarized Caco-2 cell line. PLoS Negl. Trop. Dis. 14, e0008863. https://doi.org/10.1371/journal.pntd.0008863

Moraga-Fernández, A., Ruiz-Fons, F., Habela, M.A., Royo-Hernández, L., Calero-Bernal, R., Gortazar, C., de la Fuente, J., Fernández de Mera, I.G., 2021. Detection of new Crimean–Congo haemorrhagic fever virus genotypes in ticks feeding on deer and wild boar, Spain. Transbound. Emerg. Dis. 68, 993–1000. https://doi.org/10.1111/tbed.13756

Mosammaparast, N., McAdam, A.J., 2013. Real-Time Nucleic Acid Quantification, in: Tang, Y.-W., Stratton, C.W. (Eds.), Advanced Techniques in Diagnostic Microbiology. Springer US, Boston, MA, pp. 345–353. https://doi.org/10.1007/978-1-4614-3970-7_19

Munderloh, U.G., Kurtti, T.J., 1989. Formulation of medium for tick cell culture. Exp. Appl. Acarol. 7, 219–229. https://doi.org/10.1007/BF01194061

Navarro, E., Serrano-Heras, G., Castaño, M.J., Solera, J., 2015. Real-time PCR detection chemistry. Clin. Chim. Acta 439, 231–250. https://doi.org/10.1016/j.cca.2014.10.017

Negredo, A., de la Calle-Prieto, F., Palencia-Herrejón, E., Mora-Rillo, M., Astray-Mochales, J., Sánchez-Seco, M.P., Bermejo Lopez, E., Menárguez, J., Fernández-Cruz, A., Sánchez-Artola, B., Keough-Delgado, E., Ramírez de Arellano, E., Lasala, F., Milla, J., Fraile, J.L., Ordobás Gavín, M., Martinez de la Gándara, A., López Perez, L., Diaz-Diaz, D., López-García, M.A., Delgado-Jimenez, P., Martín-Quirós, A., Trigo, E., Figueira, J.C., Manzanares, J., Rodriguez-Baena, E., Garcia-Comas, L., Rodríguez-Fraga, O., García-

Arenzana, N., Fernández-Díaz, M.V., Cornejo, V.M., Emmerich, P., Schmidt-Chanasit, J., Arribas, J.R., 2017. Autochthonous Crimean–Congo Hemorrhagic Fever in Spain. N. Engl. J. Med. 377, 154–161. https://doi.org/10.1056/NEJMoa1615162

Negredo, A., Habela, M.Á., Ramírez de Arellano, E., Diez, F., Lasala, F., López, P., Sarriá, A., Labiod, N., Calero-Bernal, R., Arenas, M., Tenorio, A., Estrada-Peña, A., Sánchez-Seco, M.P., 2019. Survey of Crimean-Congo Hemorrhagic Fever Enzootic Focus, Spain, 2011–2015. Emerg. Infect. Dis. 25, 1177–1184. https://doi.org/10.3201/eid2506.180877

Negredo, Anabel, Sánchez-Arroyo, R., Díez-Fuertes, F., de Ory, F., Budiño, M.A., Vázquez, A., Garcinuño, Á., Hernández, L., de la Hoz González, C., Gutiérrez-Arroyo, A., Grande, C., Sánchez-Seco, P., 2021. Fatal Case of Crimean-Congo Hemorrhagic Fever Caused by Reassortant Virus, Spain, 2018. Emerg. Infect. Dis. 27, 1211–1215. https://doi.org/10.3201/eid2704.203462

Negredo, Ana, Sánchez-Ledesma, M., Llorente, F., Pérez-Olmeda, M., Belhassen-García, M., González-Calle, D., Sánchez-Seco, M.P., Jiménez-Clavero, M.Á., 2021. Retrospective Identification of Early Autochthonous Case of Crimean-Congo Hemorrhagic Fever, Spain, 2013. Emerg. Infect. Dis. 27, 1754–1756. https://doi.org/10.3201/eid2706.204643

Palomar, A.M., Portillo, A., Mazuelas, D., Roncero, L., Arizaga, J., Crespo, A., Gutiérrez, Ó., Márquez, F.J., Cuadrado, J.F., Eiros, J.M., Oteo, J.A., 2016. Molecular analysis of Crimean-Congo hemorrhagic fever virus and Rickettsia in Hyalomma marginatum ticks removed from patients (Spain) and birds (Spain and Morocco), 2009–2015. Ticks Tick-Borne Dis. 7, 983–987. https://doi.org/10.1016/j.ttbdis.2016.05.004

Palomar, A.M., Portillo, A., Santibáñez, P., Mazuelas, D., Arizaga, J., Crespo, A., Gutiérrez, Ó., Cuadrado, J.F., Oteo, J.A., 2013. Crimean-Congo Hemorrhagic Fever Virus in Ticks from Migratory Birds, Morocco1. Emerg. Infect. Dis. 19, 260–263. https://doi.org/10.3201/eid1902.121193

Palomar, A.M., Portillo, A., Santibáñez, S., García-Álvarez, L., Muñoz-Sanz, A., Márquez, F.J., Romero, L., Eiros, J.M., Oteo, J.A., 2017a. Molecular (ticks) and serological (humans) study of Crimean-Congo hemorrhagic fever virus in the Iberian Peninsula, 2013-2015. Enferm. Infecc. Microbiol. Clin. 35, 344–347. https://doi.org/10.1016/j.eimc.2017.01.009

Palomar, A.M., Portillo, A., Santibáñez, S., García-Álvarez, L., Muñoz-Sanz, A., Márquez, F.J., Romero, L., Eiros, J.M., Oteo, J.A., 2017b. Molecular (ticks) and serological (humans) study of Crimean-Congo hemorrhagic fever virus in the Iberian Peninsula, 2013-2015. Enferm. Infecc. Microbiol. Clin. 35, 344–347. https://doi.org/10.1016/j.eimc.2017.01.009

Paragas, J., Whitehouse, C.A., Endy, T.P., Bray, M., 2004. A simple assay for determining antiviral activity against Crimean-Congo hemorrhagic fever virus. Antiviral Res. 62, 21–25. https://doi.org/10.1016/j.antiviral.2003.11.006

Portillo, A., Palomar, A.M., Santibáñez, P., Oteo, J.A., 2021. Epidemiological Aspects of Crimean-Congo Hemorrhagic Fever in Western Europe: What about the Future? Microorganisms 9, 649. https://doi.org/10.3390/microorganisms9030649

Rückert, C., 2014. Alphavirus and flavivirus infection of Ixodes tick cell lines: an insight into tick antiviral immunity.

Saksida, A., Duh, D., Wraber, B., Dedushaj, I., Ahmeti, S., Avšič-Županc, T., 2010. Interacting Roles of Immune Mechanisms and Viral Load in the Pathogenesis of Crimean-Congo Hemorrhagic Fever. Clin. Vaccine Immunol. 17, 1086–1093. https://doi.org/10.1128/CVI.00530-09

Salata, C., Monteil, V., Karlberg, H., Celestino, M., Devignot, S., Leijon, M., Bell-Sakyi, L., Bergeron, É., Weber, F., Mirazimi, A., 2018. The DEVD motif of Crimean-Congo hemorrhagic fever virus nucleoprotein is essential for viral replication in tick cells. Emerg. Microbes Infect. 7, 1–5. https://doi.org/10.1038/s41426-018-0192-0

Salvati, M.V., Salaris, C., Monteil, V., Del Vecchio, C., Palù, G., Parolin, C., Calistri, A., Bell-Sakyi, L., Mirazimi, A., Salata, C., 2021. Virus-Derived DNA Forms Mediate the Persistent Infection of Tick Cells by Hazara Virus and Crimean-Congo Hemorrhagic Fever Virus. J. Virol. 95, e01638-21. https://doi.org/10.1128/JVI.01638-21

Sánchez-Seco, M.P., Sierra, M.J., Estrada-Peña, A., Valcárcel, F., Molina, R., de Arellano, E.R., Olmeda, A.S., San Miguel, L.G., Jiménez, M., Romero, L.J., Negredo, A., 2022. Widespread Detection of Multiple Strains of Crimean-Congo Hemorrhagic Fever Virus in Ticks, Spain. Emerg. Infect. Dis. 28, 394–402. https://doi.org/10.3201/eid2802.211308

Shahhosseini, N., Wong, G., Babuadze, G., Camp, J.V., Ergonul, O., Kobinger, G.P., Chinikar, S., Nowotny, N., 2021. Crimean-Congo Hemorrhagic Fever Virus in Asia, Africa and Europe. Microorganisms 9, 1907. https://doi.org/10.3390/microorganisms9091907

Shepherd, A.J., Swanepoel, R., Leman, P.A., Shepherd, S.P., 1986. Comparison of methods for isolation and titration of Crimean-Congo hemorrhagic fever virus. J. Clin. Microbiol. 24, 654–656. https://doi.org/10.1128/jcm.24.4.654-656.1986

Spengler, J.R., Bente, D.A., Bray, M., Burt, F., Hewson, R., Korukluoglu, G., Mirazimi, A., Weber, F., Papa, A., 2018. Second International Conference on Crimean-Congo Hemorrhagic Fever. Antiviral Res. 150, 137–147. https://doi.org/10.1016/j.antiviral.2017.11.019

Spengler, J.R., Bergeron, É., Spiropoulou, C.F., 2019. Crimean-Congo hemorrhagic fever and expansion from endemic regions. Curr. Opin. Virol., Emerging viruses: intraspecies transmission • Viral Immunology 34, 70–78. https://doi.org/10.1016/j.coviro.2018.12.002

Spengler, J.R., Estrada-Peña, A., 2018. Host preferences support the prominent role of Hyalomma ticks in the ecology of Crimean-Congo hemorrhagic fever. PLoS Negl. Trop. Dis. 12, e0006248. https://doi.org/10.1371/journal.pntd.0006248

Spengler, J.R., Patel, J.R., Chakrabarti, A.K., Zivcec, M., García-Sastre, A., Spiropoulou, C.F., Bergeron, É., 2015. RIG-I Mediates an Antiviral Response to Crimean-Congo Hemorrhagic Fever Virus. J. Virol. 89, 10219–10229. https://doi.org/10.1128/JVI.01643-15

Surtees, R., Dowall, S.D., Shaw, A., Armstrong, S., Hewson, R., Carroll, M.W., Mankouri, J., Edwards, T.A., Hiscox, J.A., Barr, J.N., 2016. Heat Shock Protein 70 Family Members Interact with Crimean-Congo Hemorrhagic Fever Virus and Hazara Virus Nucleocapsid Proteins and Perform a Functional Role in the Nairovirus Replication Cycle. J. Virol. 90, 9305–9316. https://doi.org/10.1128/JVI.00661-16

Talactac, M.R., Hernandez, E.P., Hatta, T., Yoshii, K., Kusakisako, K., Tsuji, N., Tanaka, T., 2021. The antiviral immunity of ticks against transmitted viral pathogens. Dev. Comp. Immunol. 119, 104012. https://doi.org/10.1016/j.dci.2021.104012

Vieira Lista, M.C., Belhassen-García, M., Vicente Santiago, M.B., Sánchez-Montejo, J., Pedroza Pérez, C., Monsalve Arteaga, L.C., Herrador, Z., del Álamo-Sanz, R., Benito, A., Soto López, J.D., Muro, A., 2022. Identification and Distribution of Human-Biting Ticks in Northwestern Spain. Insects 13, 469. https://doi.org/10.3390/insects13050469

Wacker, M.J., Godard, M.P., 2005. Analysis of One-Step and Two-Step Real-Time RT-PCR Using SuperScript III. J. Biomol. Tech. JBT 16, 266–271.

Weisheit, S., 2014. Transcriptomic and proteomic analysis of arbovirus-infected tick cells.

Whitehouse, C.A., 2004. Crimean–Congo hemorrhagic fever. Antiviral Res. 64, 145–160. https://doi.org/10.1016/j.antiviral.2004.08.001

Wikel, S.K., 2018. Ticks and Tick-Borne Infections: Complex Ecology, Agents, and Host Interactions. Vet. Sci. 5, 60. https://doi.org/10.3390/vetsci5020060

Xia, H., Beck, A.S., Gargili, A., Forrester, N., Barrett, A.D.T., Bente, D.A., 2016. Transstadial Transmission and Long-term Association of Crimean-Congo Hemorrhagic Fever Virus in Ticks Shapes Genome Plasticity. Sci. Rep. 6, 35819. https://doi.org/10.1038/srep35819

Young, P.R., Ng, L.F.P., Hall, R.A., Smith, D.W., Johansen, C.A., 2014. 14 - Arbovirus Infections, in: Farrar, J., Hotez, P.J., Junghanss, T., Kang, G., Lalloo, D., White, N.J. (Eds.), Manson's Tropical Infectious Diseases (Twenty-Third Edition). W.B. Saunders, London, pp. 129-161.e3. https://doi.org/10.1016/B978-0-7020-5101-2.00015-7

Zhang, Yanfang, Shen, S., Fang, Y., Liu, J., Su, Z., Liang, J., Zhang, Z., Wu, Q., Wang, C., Abudurexiti, A., Hu, Z., Zhang, Yujiang, Deng, F., 2018. Isolation, Characterization, and Phylogenetic Analysis of Two New Crimean-Congo Hemorrhagic Fever Virus Strains from the Northern Region of Xinjiang Province, China. Virol. Sin. 33, 74–86. https://doi.org/10.1007/s12250-018-0020-7

Zivcec, M., Scholte, F.E.M., Spiropoulou, C.F., Spengler, J.R., Bergeron, É., 2016. Molecular Insights into Crimean-Congo Hemorrhagic Fever Virus. Viruses 8, 106. https://doi.org/10.3390/v8040106

Appendix

Medium preparation for tick cell culture

The preparation of all mediums used for tick cell growth and maintenance was performed under the guidelines of Munderloh and Kurtti, (1989). Each medium was kept at 4ºC and was used up to 4 months after preparation. Work was performed under a Class I Biosafety Cabinet.

L15 medium preparation.

L15 medium was used for ISE6, HAE/CTVM9 and HLE/LULS42 cells growth. Table 5 lists all the ingredients and quantities used to make a batch of 100mL of L15.

Table 5. Ingredients for L15 medium

Ingredients	
L15	68 mL
Tryptose phosphate broth 10%	10 mL
Fetal bovine serum 20%	20 mL
2 mM L-glutamine	1 mL
2 mM Pen/strep	1 mL

MEM with Hank's salts medium preparation

MEM with Hank's salts was used for ISE6, and HLE/LULS42 cells growth. Table 6 lists all the ingredients and quantities used to make a batch of 100mL of L15B.

Table 6. Ingredients for MEM with Hank´s salts

Ingredients	
MEM with Hank's salts	68 mL
Tryptose phosphate broth 10%	10 mL
Fetal bovine serum 20%	20 mL
2 mM L-glutamine	1 mL
2 mM Pen/strep	1 mL

L15B complete medium preparation.

L15B medium was used in HAE/CTVM9 cell growth. Table 7 lists all the ingredients and quantities used to make a batch of 100mL of L15B.

Table 7. Ingredients for L15B complete

Ingredients	
L15B initial	82 mL
Tryptose phosphate broth 10%	10 mL
Fetal bovine serum 5%	5 mL
Lipoprotein	1 mL
2 Mm L-glutamine	1 mL
2 Nm Pen/Strep	1 mL
1 M NaOH	200 uL

L15B initial medium preparation.

L15B initial was necessary to produce the L15B medium. The vitamin stock solution and the mineral stock solutions had previously been prepared, aliquoted and stored at -80ºC. To make 1 L of L15B initial, L-15 (Leibovitz) powder is dissolved in 900µL of deionised water in an Erlenmeyer. Then, is supplemented with the ingredients listed on Table 8. Deionised water is added to a final volume of 1L. The medium is filtrated (0.22 µm) and stored up to six months in 4ºC.

Table 8. Ingredients for L15B initial.

Ingredients	
L-aspartic acid	299 mg
L-glutamic acid	500 mg
L-proline	300 mg
α-ketoglutaric acid	299 mg
D-glucose	2239 mg
Vitamin stock	1 mL
Mineral stock	1 mL

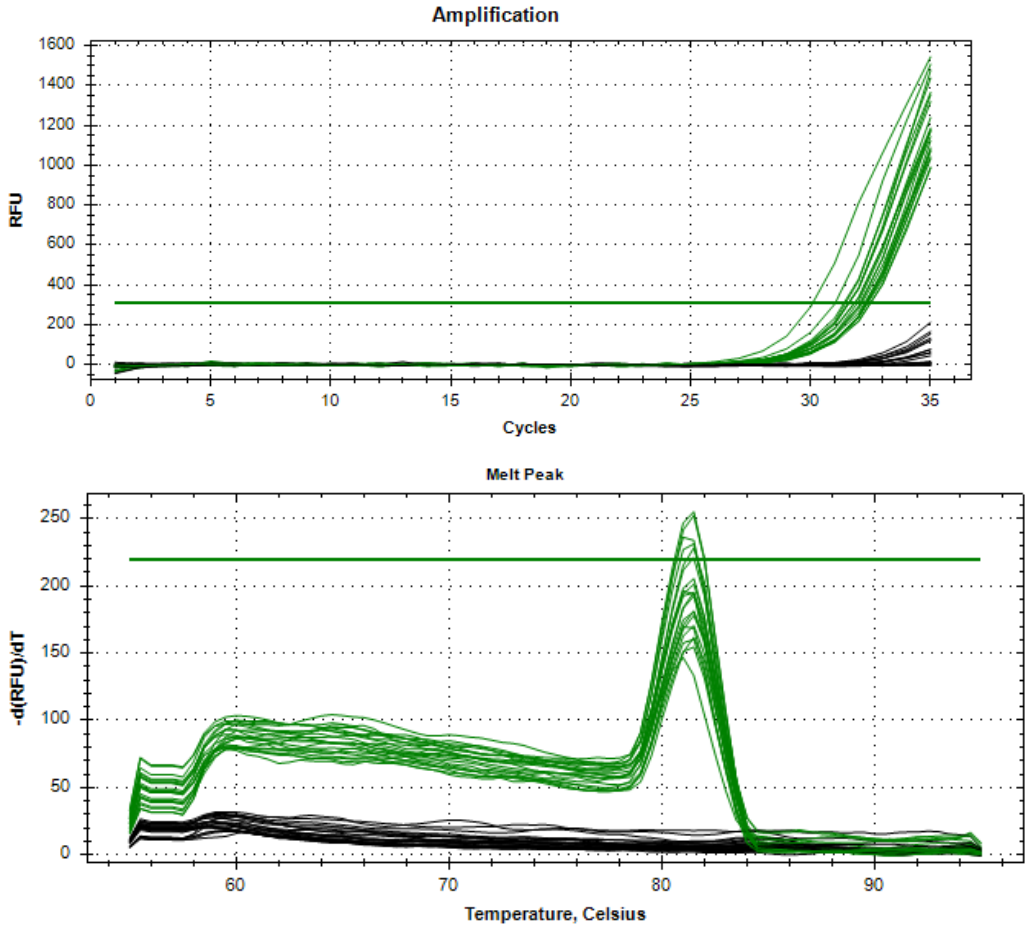

Figure 22. SYBR Green amplification plot, and respective melt-curve, of the temperature gradient analysis. A temperature gradient ranging from 55ºC to 65ºC was used in this qPCR. The primer concentration is the reaction was 400 nM. Green lines represent gBlocks® amplification, and the black lines represent the negative control of the reaction. The quantification cycle (Cq) values obtained for each different temperature tested are very similarly, and, visually, show no difference.

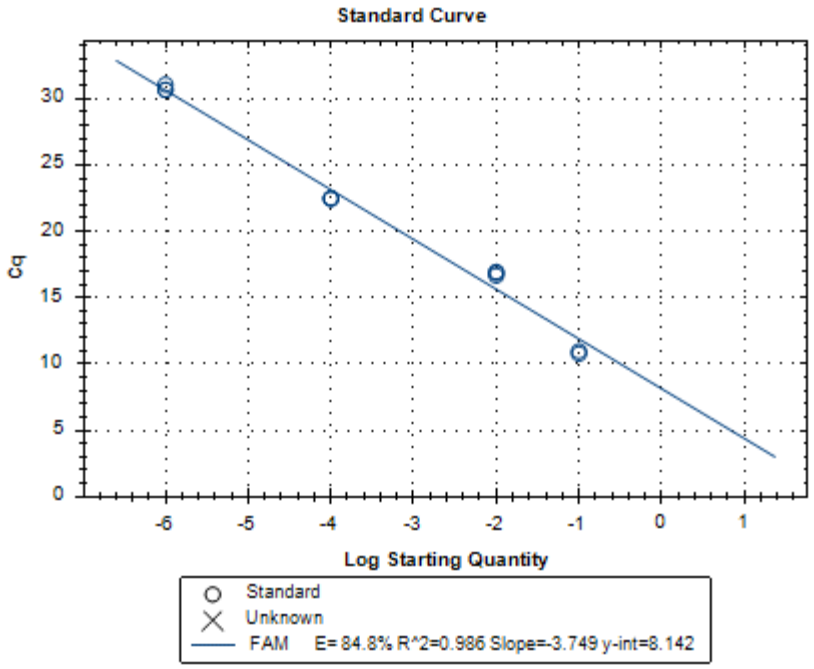

Figure 23. Standard curve used for all HAZV quantification in tick cells. It was decided to use the same standard curve throughout all the HAZV RNA analysis by RT-qPCR. This decision was made to reduce costs and to maximise the extent of RNA samples analysed in the PCR plate in each assay. The present standard curve was made using 10 fold serial dilutions of gBlocks®. The cycling conditions used were the same as for the RNA analysis (indicated in Table 2).

Table 9. Statistical analysis on the viral titres obtained for the different tick cell lines, for each MOI. All samples were tested using the Ordinary one-way Anova multiple comparisons test. The samples for which the *P-value* was smaller than 0.05 were considered significative and are displayed in the table.

MOI 1:10

Tukey's multiple comparisons test	Mean Diff,	95,00% CI of diff,	P Value
HLE/LULS42 6 dpi vs. ISE6 6 dpi	2,019	0,04455 to 3,994	0,0417
HLE/LULS42 8 dpi vs. ISE6 8 dpi	2,93	0,9550 to 4,904	0,0007
HLE/LULS42 10 dpi vs. ISE6 10 dpi	3,088	1,113 to 5,063	0,0003
HLE/LULS42 30 dpi vs. ISE6 30 dpi	2,257	0,2819 to 4,231	0,0151
HLE/LULS42 8 dpi vs. HAE/CTVM9 8 dpi	2,358	0,3833 to 4,333	0,0097
HLE/LULS42 10 dpi vs. HAE/CTVM9 10 dpi	2,209	0,2348 to 4,184	0,0186

MOI 1:1

Tukey's multiple comparisons test	Mean Diff,	95,00% CI of diff,	P Value
HLE/LULS42 6 dpi vs. ISE6 6 dpi	2,762	1,391 to 4,133	<0,0001
HLE/LULS42 8 dpi vs. ISE6 8 dpi	2,231	0,6981 to 3,764	0,001
HLE/LULS42 10 dpi vs. ISE6 10 dpii	2,286	0,9150 to 3,657	0,0001
HLE/LULS42 60 dpi vs. ISE6 10 dpii	3,87	2,499 to 5,241	<0,0001
HLE/LULS42 4 dpi vs. HAE/CTVM9 4 dpi	1,934	0,5630 to 3,305	0,0014
HAE/CTVM9 8 dpi vs. ISE6 8 dpi	1,707	0,3362 to 3,078	0,0063

MOI 5:1

Tukey's multiple comparisons test	Mean Diff,	95,00% CI of diff,	P Value
HLE/LULS42 60 dpi vs. ISE6 60 dpi	2,12	0,2410 to 3,999	0,0172
HLE/LULS42 4 dpi vs. HAE/CTVM9 4 dpi	2,322	0,4436 to 4,201	0,0067